DEVELOPMENT OF OCTA AUTOMATED SEGMENTATION AND MEASUREMENT TOOLS FOR ASSESSMENT OF CEREBROVASCULAR AND NEURAL HEALTH IN AGING POPULATIONS

SAFA TANZEEM

Thesis submitted to the University of Ottawa
in partial Fulfillment of the requirements for the
Master of Applied Science in Electrical and Computer Engineering

Ottawa-Carleton Institute for Electrical and Computer Engineering
Faculty of Engineering
University of Ottawa

Abstract

Cerebral small vessel disease (CSVD) is one of the most commonly occurring vascular disease in the older population. Research has shown that the emergence of cerebrovascular disease has a profound effect on the changes that occurs in retinal vasculature. Optical coherence tomography angiography (OCTA) is a non-invasive, high resolution imaging modality used to extract images of retinal vasculature. However, manual segmentation of these images requires experienced clinical expert and is highly subjective to the individual's background. Therefore, there is a need of developing an automated segmentation technique for OCTA images.

This research proposes a novel approach for automatic segmentation of OCTA images. The OCTA scans in this study involved individuals from two groups, older individuals whose scans were obtained from a publicly available dataset ROSE-1 [1], and OCT images of younger individuals that were acquired in the lab at University of Ottawa called NCM images. The proposed approach comprises of pixel-level and centerline level segmentation of OCTA images using Attention UNet model of different depths and merging these images to form a fully segmented superficial vascular complex (SVC) OCTA image. The experimental results demonstrates that the proposed approach (for fully segmented SVC OCTA) provides an accuracy of 0.9188, average dice of 0.7853, kappa score of 0.7354, G-mean score of 0.847 and balance accuracy of 0.85518. The trained pixel-level segmentation model was again used to segment NCM images, and the resulting segmented image was overlapped over the original image and studied.

Subsequently, pixel-level segmented images were used to extract vascular features from retina such as vessel density, vessel length density, vessel perimeter index and vessel mean diameter for both the groups. It was found that there is a decrease in mean diameter of blood vessels (p-value < 0.05) in older individuals as compared to the younger group while the other parameters were not statistically significant (p-value > 0.05).

Dedication

Dedicated to my husband: Kunwar Rehan, parents: Tanzeem Akhtar & Kahkashan Parveen, my siblings and my nieces.

Acknowledgements

I would like to thank my supervisor Dr. Jason Steffener for his guidance and support during my master's program. Our biweekly discussions helped shape this work and prompted me to develop new ideas and breakthroughs. A special thanks goes to my colleague Dylan Franklin for providing support in the lab. I also want to thank the numerous participants that provided the samples for the research, taking time out of their schedule and being patient with the imaging process.

I would also like to thank my husband, Kunwar Rehan and my family for their unwavering encouragement and support. They have stood by me through my entire academic journey and have relentlessly been a dependable force in my life throughout.

Table of Contents

List of Figures

List of Tables

List of Abbreviations

ADAS	Alzheimer's Disease Assessment Scale
AG	Attention Gate
CMB	Cerebral Microbleed
CS Net	Curvilinear structure Segmentation Network
CSVD	Cerebral Small Vessel Disease
CSF	Cerebrospinal Fluid
CT	Computer Tomography
DVC	Deep Vascular Complex
FN	False Negative
FP	False Positive
ILM	Internal Limiting Membrane
IPL	Inner Plexiform Layer
IPN	Image Projection Network
MMSE	Mini-Mental State Exam
MRI	Magnetic Resonance Imaging
OCTA	Optical Coherence Tomography Angiography
OPL	Outer Plexiform Layer
PET	Positron Emission Tomography
ROSE	Retinal OCT-Angiography Vessel Segmentation Dataset
SCP	Superficial Capillary Plexus
SD-OCT	Spectral Domain Optical Coherence Tomography
SVC	Superficial Vascular Complex
TD-OCT	Time Domain Optical Coherence Tomography

TN	True Negative
TNR	True Negative Rate
TP	True Positive
TPR	True Positive Rate
VGG	Visual Geometry Group
WMH	White Matter Hyperintensity

Chapter 1

Introduction

Cerebrovascular diseases are a leading cause of death and life altering disability in the world. Cerebral small vessel disease (CSVD) is the most commonly occurring vascular disease in the aging population. Its early detection highly depends on the neuroimaging techniques indicating morphological changes in the brain [2]. Therefore, in addition to the brain images there is a need to identify potential biomarkers from other organs in the body which can signal changes occurring in the blood vessels. This information can aid in the early detection of these diseases, so that the necessary care can be provided.

Being an extension of the brain, retina shares the same anatomic, embryologic, and physiologic characteristics as the brain. Anatomically, the internal carotid artery supplies blood to both the anterior brain and retina. Embryologically, the forebrain neuroectoderm contributes to the development of cerebrum as well as the retinal pigment epithelium layer and the neural retina [3]. Various studies have showed that retina provides a window to the cerebrovascular and neural health of the brain [3] [4] [5]. The changes in the brain have been linked to the changes in the eye which can vary from the alteration in the vision, structural and functional changes. Previously, optical coherence tomography and retinal fundus were being used for the research, until the development of a new imaging modality known as optical coherence tomography angiography (OCTA). It is a non-invasive imaging modality which provides vascular information of the retina not available before. Hence, it raises the opportunity to develop tools which will aid in the early detection of microvascular changes *in vivo*.

1.1 Problem Definition

The objectives of this research are as defined in this section. The goal is to develop an automated segmentation tool for the OCTA scans and extract vascular features (biomarkers) which can be linked to the changes in the brain as the person ages or develops diseases associated with ageing such as cerebral small vessel disease (CSVD) leading to cognitive decline. To achieve this objective, it was essential to collect some OCTA scans of younger individuals for comparison. Consequently, proper training was obtained for this purpose and some OCTA images were collected in the lab of University of Ottawa.

1.2 Motivation

With the development of optical coherence tomography angiography (OCTA) imaging technology, which is a non-invasive, reliable and produces high resolution images of retinal vasculature, appropriate vascular features can be extracted from the retina. These features along with the connection of eye to the brain has intrigued researchers to investigate the retinal vascular abnormalities a person develops with aging which leads to cognitive decline and cerebral small vessel diseases[6][7][8][9] . Recent studies show, the high-resolution OCTA images have a great potential in detection of brain diseases associated with ageing such as CSVD, dementia and stroke [4][5][10] and when combined with deep learning may provide a potential tool to automate the detection and quantification of microvascular changes due to underlying brain diseases.

Despite all this research, there is a lack in consensus of a standard automated segmentation tool for the OCTA scans which can segment images accurately. Manual segmentation is a time-consuming process as it requires interrater and intra-rater reliability to ensure that the segmentation performed are not subjective to an individual rater. Furthermore, manual segmentation involves experienced clinical experts to perform them individually for each image. In contrast, for automated segmentation involving deep learning techniques once the model is trained with OCTA and ground truth images, it will automatically segment any other OCTA image and does not require the

presence of an expert for each image. Therefore, most of the work done in this research aims in developing a good segmentation approach for the superficial vascular complex (SVC) OCTA images. A good quality segmentation of the retinal vasculature in OCTA images is important as it facilitates precise extraction of features which might aid in the early detection and treatment of diseases like CSVD, Alzheimer's, dementia etc.

1.3 Thesis Roadmap

This thesis covers the wide range of work that has been done during the research from the acquisition of images, to developing a segmentation tool, extracting vascular biomarkers and analyzing them. The organization of this thesis is discussed in this section as follows:

Chapter 2 builds the background of the work that has been presented in the subsequent chapters. It starts with the description of cerebral small vessel disease (CSVD) and its neuroimaging features. A description of the association between retina and the brain is mentioned. Subsequently, a review of the changes in retinal vasculature with the change in brain is described. Finally, a detailed overview of the segmentation of the OCTA scans is done. This chapter puts into perspective the rest of the work that has been done during this research.

Chapter 3 presents the methodology used in this research. It describes the acquisition of the image and a detailed description of the image processing techniques that has been used. The proposed SVC OCTA segmentation approach has also been discussed in this chapter. This is followed by the description of the vascular features that has been extracted.

Chapter 4 presents a series of results of the methodology described in chapter 3. It also discusses the features extracted and the findings of this study.

Chapter 5 summarizes the work done during this research. It also presents the limitation and the work that can be done in future.

Chapter 2

Background and Related work

This chapter builds the background of the work that has been done in this study. It starts with a description of cerebral small vessel disease and the neuroimaging features and symptoms associated with it. Subsequently, the connection between the brain and the eye is described followed by how OCTA can aid in detecting brain related biomarkers in the eyes. A survey of the work similar to what has been done in this research is also presented. Finally, an overview of the OCTA segmentation techniques used by the researchers has been discussed.

2.1 Cerebral Small Vessel Disease (CSVD)

Cerebral small vessel disease refers to several diseases that are caused by the abnormalities or structural change in the small vessels of the brain. Current definition of small vessel identifies all vascular structures varying from small arteries, capillaries, arterioles, venules, and small veins in the brain with a diameter of 50-400 μm [11][12].

Various studies have linked small vessel disease with cognitive decline, Alzheimer's, dementia, and Parkinson's disease [13]. It is a cause for nearly 25% of the ischemic strokes and 45% of dementia [11]. It's diagnosis is done through MRI and CT scans. [11][12].

2.1.1 Neuroimaging Features of CSVD:

The neuroimaging features related to CSVD are described as follows:

1. **Recent small Subcortical Infarcts**

   This is a result of a severe ischemia of a single perforating artery and is identified by the lesions with less than 20mm diameter developing around the arteriole region within a few weeks. These lesions are round or ovoid in shape and are present in the white matter, brainstem, or basal ganglia. Diffusion weighted imaging is an imaging technology most sensitive to these

lesions. It has been observed that more than one third of the lesions recovered completely with no residual cavities and 40% were located adjacent or within the white matter lesions. [11]

2. **Lacunar Infarct**

It is a small round fluid filled cavity with a diameter between 3-15mm. The fluid has a similar signal to that of cerebrospinal fluid (CSF). It has been classified in different ways by different people. Based on the formation, Poirier and colleagues [11] classified the lacunas into three categories namely, Subtype I, subtype II, and subtype III. Subtype I are formed after old lacunar infarction, subtype II is formed after old hemorrhagic lesions and subtype III are secondary to enlarged perivascular spaces. It has also been classified based on their shape in an MRI by Herve and colleagues [11] as Slab, stick ovoid, multiple components. They also showed that around 83% lacunar infarcts are ovoid in shape. It may occur adjacent, isolated, or fused in white matter hyperintensity. [11]

3. **White Matter Hyperintensities (WMH)**

It includes wide-ranging expressions such as disruptions of small blood vessels, small infarcts present in white matter, reduced cerebral flow, glial activation etc. It is identified as symmetrical hyperintensities in T2 weighted MRI. Diffusion tensor MRI and Magnetization transfer MRI are used to study the white matter present in the brain, it also helps in differentiating WMH with other lesions such as lacuna and atrophy and helps in studying the relation between white matter and dementia. [11]

4. **Microbleeds**

The microbleeds are small signal void of around 2-5mm but can be up to 10 mm in size that are caused by previous hemorrhages. Depending on the location of the lesions it can be classified into three categories: lobar, deep, subtentorial CMBs. The deep and subtentorial microbleeds results in declining motor speed where as lobar microbleed result in declining

executive and memory functions. These lesions usually appear in paramagnetic sensitive MR sequence and not on CT scans, T1 and T2 weighted MR sequence. [11]

5. **Brain Atrophy**

   It is referred to a condition when the volume of the brain decreases without any brain injury. It usually cooccurs with white matter hyperintensities in elder people and has been associated with dementia and cognitive decline. Brain atrophy can be characterised by reduced total volume of brain, decrease in white matter volume, decrease in gray matter volume, increased ventricle volume. Some studies have found a linear relation between WMH and brain atrophy and have stated that the increase in one lead to an increase in other as well. [11]

2.1.2 Symptoms of CSVD

A person with CSVD may or may not develop symptoms such as hallucination, agitation, sleep disturbances, appetite changes, apathy, and irritability [11] depending on the severity of the disease (mild, moderate, or severe). Individuals who show no symptoms of CSVD but have been diagnosed with it (especially with mild SVD) are called 'silent' SVD. The problems that have been associated with CSVD are discussed as follows:

- Cognitive impairment: Studies [14] have shown that an increase in white matter lesions and lacunar infarcts have been associated with a decrease in Mini Mental State Examination (MMSE) and Alzheimer Disease Assessment Scale (ADAS) score.
- Depression: It has been linked to having CSVD [15], especially if the older person has developed depression for the first time in his or her life.
- Dementia: Individuals suffering with CSVD have been linked to people having dementia or developing it later [11] [16].
- Strokes: CSVD leads for up to 25% of the ischemic stroke and increases the chances of having it by two folds [11][16].

- Problem with walking or balancing: Several studies [11][17] have found the contribution of increased White Matter Lesion progression in gait decline.
- Neuropsychiatric Symptoms: This includes hallucination, agitation, sleep disturbance, appetite change, irritability etc.[11]

2.2 Eye and the Brain

The detection of CSVD is challenging even with MRI as it studies the changes that have occurred in the cerebra due to ischemia and does not visualize the blood vessels. In other words, it measures the damage to the brain which happens as a result of vascular damage. To measure the blood vessel changes through MRI, a contrast material called gadolinium is injected through the arm making it invasive. The resulting image has low spatial resolution as compared to the high-resolution retinal vascular scans produced through OCTA. Since retina is embryologically linked with the brain [3][18] and the internal carotid artery supplies blood to the brain and eye [19], researchers have been intrigued about the possibility of finding biomarkers of CSVD within retina. The most used retinal imaging technology is Color fundus; however, it is difficult to study the retinal microvasculature through the color fundus images. Fluorescein angiography is another retinal imaging technology which captures the blood flow information in a retina, a dye is injected into the vein of the person's arm and the blood flow information is captured while it passes through the blood vessels of the eye. Since, Fluorescein angiography is invasive in nature it is not recommended. The recent development of Optical coherence tomography angiography has provided researchers with a non-invasive tool to extract depth resolved blood flow information in the retina to a level which was not available before. Hence, a quick review of the OCTA imaging technology is done before diving into its application for the detection of biomarkers through retina associated with brain aging due to small vessel disease, dementia, and Alzheimer's.

2.2.1 Optical Coherence Tomography Angiography

Optical coherence tomography angiography (OCTA) is an extension of OCT; hence a brief description of OCT methodology is important to understand the working of OCTA. Optical coherence tomography (OCT) is a non-invasive, low coherence interferometric based imaging modality which uses light to capture high-resolution cross-sectional images of the retina. OCT images helps in the understanding and analysis of retinal layers. It aids in measuring the retinal thickness of different layers which facilitates the early detection of many retinal diseases [20][21]. The earlier method of capturing OCT scans was time-domain OCT (TD-OCT) in which the scans were generated by the detection of the interference signal in between the light backscattered from the biological tissue sample and the light reflected from the reference mirror. Subsequently, the position of the reference mirror is changed to obtain intensities of the backscattered light at different depths in the tissue sample. A-scans are formed by developing an intensity profile at various depths axially as shown in Figure 1(a), where as a sequence of A-scans composes a B-scan of a retina which is a result of transverse scanning in a predefined axis as shown in Figure 1(b). In spectral domain OCT (SD-OCT), the reference mirror is fixed, and a charge coupled device (CCD) is used to detect the frequency components obtained by splitting the interference pattern. The Fourier transform of the received signal is calculated and each frequency component corresponds to a depth in the tissue yielding in the accumulation of all the points in an A-scan simultaneously, hence increasing the speed. A B-scan is acquired similarly as in TD-OCT by obtaining A-scans along the traverse plane [22]. An SD-OCT allows 20,000-40,000 A-scans per second, which allows an imaging resolution of ~3-5 microns as compared to 10-15 microns in TD-OCT which allowed only ~400 A-scans per second [23]. With the development of SD-OCT which ensures high speed and resolution, OCT became an important tool in both qualitative and quantitative assessment of tissue in the field of ophthalmology.

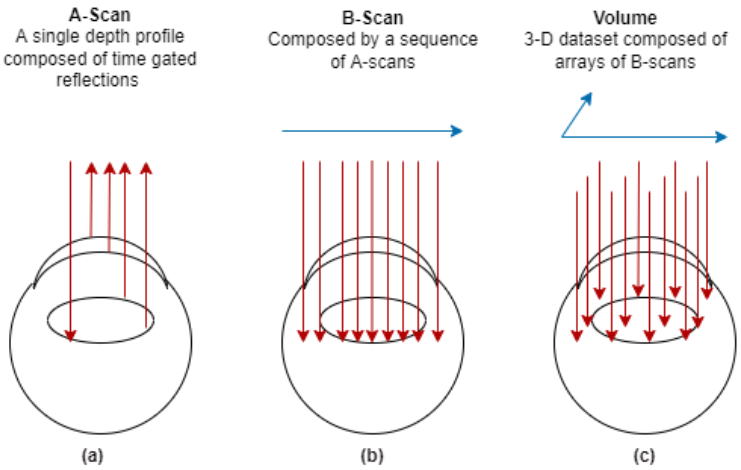

Figure 1: Representation of OCT (a) A-scan (b) B-scan (c) Volumetric scan [24]

Based on OCT, a new imaging modality was developed known as Optical coherence tomography angiography (OCTA) which allows the visualization of functional blood vessels in the eye. The OCTA images are obtained depending on the fact that everything in an imaged volume is stationary except for the blood. Therefore, it uses the changes in the successive OCT signal because of the moving particles in the retina (mostly red blood cells) as a motion contrast mechanism to map the blood vessels. Repeated cross-sectional B-scans are obtained at the same location, where one OCT scan contains the signal backscattered from the static structural tissue and the other contains the signal backscattered from the moving blood particles[23][25]. The changes in the subsequent OCT signals generates an angiographic contrast caused by the blood flow which helps in visualizing the microvasculature as shown in Figure 2. The final OCTA image is then generated by using available algorithms which either uses the OCT signal amplitude or OCT signal phase or both (known as complex amplitude).[25]

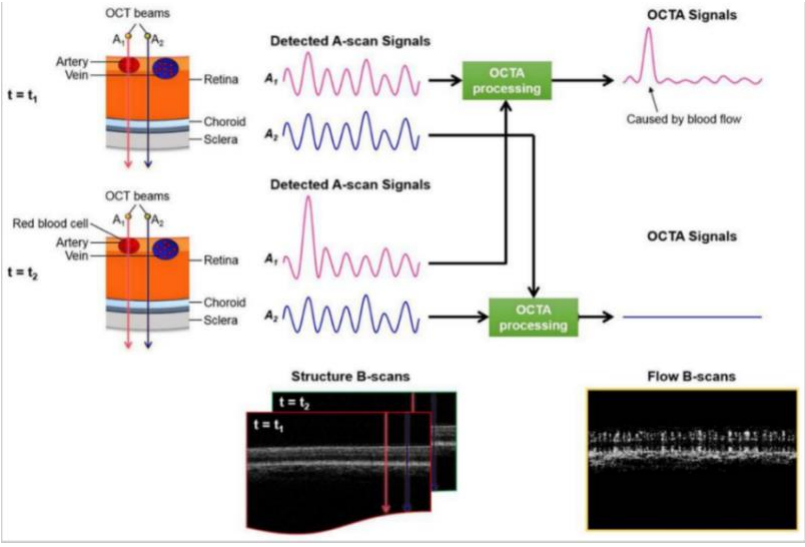

Figure 2: Depiction of OCTA image generation process (obtained from [23]**)**

The OCTA images can be captured at different retinal depths by projecting the maximum OCTA flow signals. Based on the retinal depth of capturing the OCTA image, it can be divided as Superficial Vascular Complexes (SVC), Deep vascular complexes (DVC) as shown in Figure 3 and inner retinal vascular plexus which is a combination of both SVC and DVC [1].

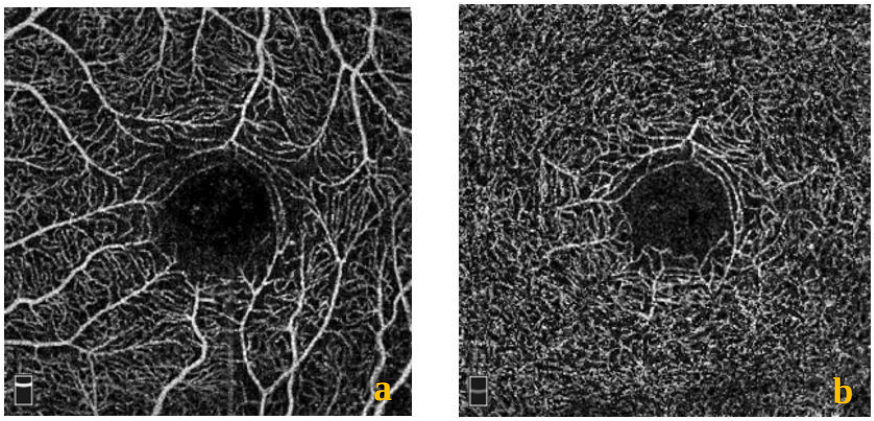

Figure 3: (a) SVC OCTA image (b) DVC OCTA image [1]

The SVC starts from 3µm below the internal limiting membrane (ILM) till 15 µm below the inner plexiform layer (IPL). Once the SVC ends, DVC starts from 15 µm below the inner plexiform layer till outer plexiform layer (OPL) [26]. The ILM, IPL and OPL can be seen from Figure 4 which

displays different retinal layers in an OCT scan. Please Note, that the images used in this study is the SVC OCTA scans.

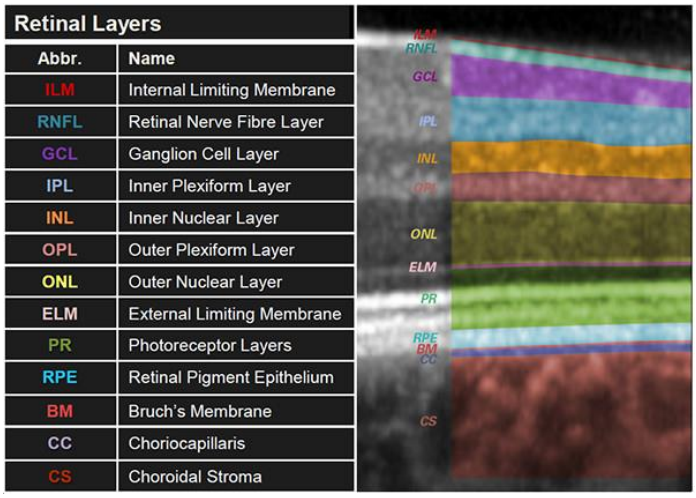

Retinal Layers	
Abbr.	Name
ILM	Internal Limiting Membrane
RNFL	Retinal Nerve Fibre Layer
GCL	Ganglion Cell Layer
IPL	Inner Plexiform Layer
INL	Inner Nuclear Layer
OPL	Outer Plexiform Layer
ONL	Outer Nuclear Layer
ELM	External Limiting Membrane
PR	Photoreceptor Layers
RPE	Retinal Pigment Epithelium
BM	Bruch's Membrane
CC	Choriocapillaris
CS	Choroidal Stroma

Figure 4: Retinal layers in an OCT scan (obtained from[27]**)**

2.2.2 Eye Parameters

The parameters which can be measured through an OCTA scan can be either vascular parameters or the foveal area zone (FAZ) parameters. The vascular parameters include vessel density, vessel length density, vessel perimeter index, mean diameter of blood vessels etc. The FAZ parameters includes FAZ area and contour irregularity of FAZ.

In recent years, several studies have analyzed the retinal microvasculature from OCTA images amongst two group, individuals with mild cognitive impairment (MCI) and Alzheimer's disease. Researchers in [28][29][6][30][31] found a decrease in the vascular density parameters such as vessel density, vessel length density etc. in group with Alzheimer's disease as compared to the group with Mild Cognitive impairment (MCI). However, a study done by Kreeke et al.[32] on OCTA images of a group with preclinical Alzheimer's patients, identified by amyloid-beta deposits (Aβ+) in the brain found that the group with Aβ+ has higher vessel density than the group with Aβ-. Additionally, two studies by Haan et al. [33] and Querques et al. [34] have shown no difference in the vascular parameters of the two group. Hence, a majority of above-mentioned studies describe

a decrease in vascular density parameters in the group with Alzheimer's disease as compared to MCI group.

Some researchers have tried to study the brain parameters and their link with the retinal vasculature as observed in OCTA images. Haan et al. [33] found an inverse relation between the vascular density and white matter hyperintensity (WMH) score (Fazekas score) indicating that fewer WMH were found in AD participants with higher vessel density. Similarly, Lahme et al. [35] observed an increased vessel density with fewer number of WMH.

Bulut M. et al. [28] found a positive correlation in between MMSE score and vascular density in Superficial OCTA scans. Better MMSE score is found in people with better cognitive ability and now has been associated with higher vascular density. Similarly, Yoon et al. [29] found decreased vessel density in AD group and has later linked this result to lower MMSE score in MCI group as compared to controls. Hence, associating increased vessel density with better cognitive functions. Zhang Y. et al. [36] also found a positive correlation in between the cognitive performance judged by Montreal cognitive assessment score and vessel density in parafoveal SCP OCTA scan.

The above-mentioned studies and their results shows great promise in the vascular parameters extracted from OCTA images and brain diseases caused due to ageing such as such as CSVD, Alzheimer's etc. However, more research is required to reach a consensus. One of the limitations of the research done to date is that the dataset of most of the research done is not publicly available with classification in between different groups. Moreover, the calculation of the mentioned parameters requires a binary segmented OCTA image. However, the segmentation of retinal vasculature of OCTA images remains a challenging task due to the complexity of the blood vessels and the artifacts present in the OCTA image. Hence, a review of the algorithms that have been used previously for the segmentation of retinal vasculature of OCTA images (for all uses) is essential to understand the best suited approach.

2.2.3 Segmentation of OCTA Images:

Based on the technique used, segmentation of OCTA images can be classified as (a) Thresholding (b) Clustering (c) Deep learning. Since the area of interest of this research is the eye, the literature considered while studying for the OCTA segmentation techniques used were based on the ocular applications. The structure of interest in the OCTA images of an eye is either the vasculature or the foveal area zone (FAZ) as seen in Figure 5.

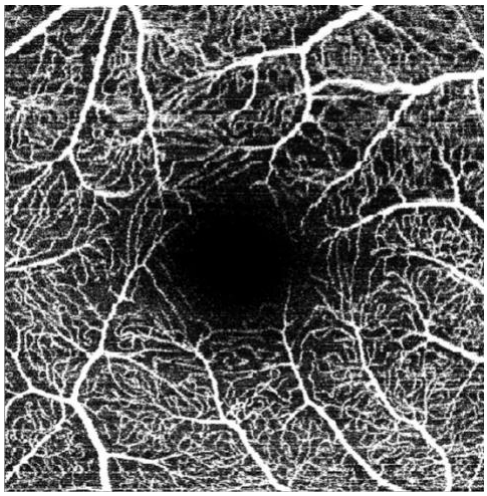

Figure 5: Example of an OCTA image with the blood vessels and FAZ area at the center

The findings of the papers reviewed according to the segmentation techniques are presented as follows:

1. Thresholding: It is a common image segmentation technique which is used to divide an image into two or more classes commonly referred as “foreground” and “background”. The criteria to determine the threshold value can be classified as global thresholding and local thresholding.

Global thresholding is where a single threshold value calculated by the image intensity histogram is used for the entire image. Several studies [37][38][39] did not clarify the final approach taken to calculate the threshold. The most common technique of calculating global threshold by minimizing or maximizing intra class intensity variance is known as Otsu’s method which have been used by numerous studies [40] [41] [42][43] for segmentation. De Jesus et al. [44] used the percentage of image intensity histogram to calculate the threshold value, this variable

threshold value made the program more robust as compared to an absolute threshold value. Another method of calculating the threshold value is by calculating the weighted average of the intensity histogram as done by Meiburger et al.[45]. Zhang et al. [46] used global thresholding as an intermediate process during segmentation.

Another type of thresholding that has been used for the OCTA segmentation is adaptive or local thresholding, where a threshold is calculated for each pixel by analyzing the image in a smaller user defined neighborhood. The threshold value is determined by calculating the first order statistics such as standard deviation or mean of the pixels within a neighborhood. Several studies [47][48] have used Phansalkar method for the adaptive thresholding where a local threshold is calculated by using average and standard deviations of a grayscale image. Zhongdi et al. [49] calculated the threshold value through local mean in the user defined neighborhood, where as., Li Su et al. [47] and Kim et al. [50] used local median to compute the threshold value. Most of the studies that have performed thresholding as the segmentation method have not provided the quantitative validation of these segmentation techniques which is important to assess the correctness of the segmented image.

Terheyden et. al. [40] compared the automated thresholding method with the manual and found that automated thresholding outperforms the manual thresholding method. Mehta et al. [51] and Terheyden et. al. [40] compared different thresholding techniques and found that the quantitative parameters obtained from different segmentation techniques cannot be interchanged. Hence, there is still a need for a standardized strategy for the segmentation of retinal vasculature.

2. Clustering: Clustering is the grouping of pixels of different classes based on a parameter. Based on a measure, it is decided that the pixel belongs to which class. In other words, clustering involves grouping of pixels with similar traits in a class. Measures based on which the decision is made are classified into two kinds namely, distance measures and similarity measures. Pixel intensity is the

most common measure used for grouping the pixels together with the help of algorithms such as k-means [52][53] or c-means clustering algorithm [54].

Engberg et. al. [55] in 2020 used a clustering-based approach to segment OCTA images. In this study, a probabilistic pixel classification method originally developed for texture segmentation was used where, the information (local features) from pre segmented data is used to train a dictionary cluster of image patches with their corresponding label. This method was able to segment the larger vessels with a Dice coefficient of 0.8200 (the comparison is made with respect to manually labelled image).

3. Deep Learning: The application of Deep learning has seen recent increased interest in the field of medical image processing. Many researchers have adopted deep learning algorithms for the segmentation and classification of medical images because they outperform the state of the art. It is because the convolutional neural networks automatically learn high-level features and use them to segment complex biomedical images by correlating each pixel to a specific class. The drawback which has prevented researchers from using this for biomedical images was the absence of large datasets for training, which has been mitigated by a great extent with the use of transfer learning [56]. Transfer learning is when the deep learning models are pre trained over a large and similar dataset. The models are then adjusted according to the region of interest.

The development of new deep learning models such as UNet has shown great promise in the field of biomedical image segmentation which typically requires localization (each pixel is assigned a class label). The most commonly used deep learning algorithms for OCTA vasculature segmentation till date are ResNet [1][57], CSNet[58], UNet [58][59][60][61][62], VGG [63] and custom-made networks.

Giarratano et. al. [58] compared the adopted version of three neural network architectures namely CNN, UNet and CS-Net along with some traditional approaches using filtered image and machine learning to segment the retinal vasculature in OCTA images. The results demonstrated

that the performance of U-Net and CS-Net outperformed the rest of the methods in nearly every evaluation metrics. Ma et. al. [1] proposed a custom split based coarse to fine vessel segmentation neural network architecture named as OCTA-Net where a preliminary confidence map of vessels is generated using the coarse segmentation module followed by a split based segmentation module which optimizes the shape of the retinal vasculature. This network has an ability to segment thin and thick vessels on their own. The authors also compared the results of their network with some existing networks such as IPAC, COSFIRE, U-Net, Res U-Net, CE-Net, DU-Net, CS-Net etc. and found that the proposed network outperforms the existing networks with a Dice score of 0.7597 for SVC, 0.7074 for DVC (when compared with manually segmented images).

Several researchers modified the most used UNet architecture to achieve the segmentation of OCTA. Lo et. al. [59] adopted UNet Architecture to segment OCTA images where a batch normalization layer was added after the convolution layer and is followed by a dropout layer. This resulted in superficial capillary plexus (SCP) segmented image with a dice score equal to 0.8599 and DVC dice score equal to 0.7986. The authors then used these segmented images to find the biomarkers for the early detection of Diabetic retinopathy (DR). Pissas et. al. [60] used a modified UNET architecture of depth equal to 3 to segment the OCTA vasculature, the convolution layer was replaced by a residual block in the network where the resolution of the input feature and output feature map were equal. The encoder side had three residual blocks out of which first two blocks were followed by a max pooling layer which divides the feature maps by a factor of two. Yu et. al. [61] also modified the UNet architecture to develop a method to reconstruct the 3D vessel segmentation of OCTA images, it is accomplished by designing a network to predict the depth of blood vessels (depth estimation) and merge that information with the 2D segmentation of OCTA images. The depth map estimation is done by customizing UNet architecture, the encoder and decoder side are kept the same but instead of using skip connections, the researchers designed a structure constraint block (SCB) block. This block is implemented after each encoder and feeds

only vessel related information to the decoder. The authors also compared the results with other state of the art approaches and found that the proposed method outperforms all other approaches for a 3D segmentation. However, this paper did not provide a validation for 2D segmentation.

Li et. al. [64] provided an improvement over previously proposed IPN architecture [63] by introducing IPN-V2 with plane perceptron and IPN-V2+ with global retaining for 3D to 2D image segmentation. These two methodologies eliminated the limitations of previously proposed IPV method. IPV was using unidirectional pooling which led to insufficient semantic information in 2D plane. Hence, in IPN-V2, UNet architecture was used as a plane perceptron which improved the segmentation performance. The other limitation of having checkerboard effect in IPN was removed by the proposed U-shaped global network which performs global retraining. The performance of the proposed network was tested over the proposed dataset of 500 images. The results of IPN-V2+ and IPN-V2 outperformed previously proposed IPN network.

2.3 Conclusion

This chapter builds the background of the thesis, starting with the brief description of CSVD and how it affects the cognitive ability of a person. Subsequently, the association between eye and the brain is discussed in detail followed by the discussion of how vascular parameters from OCTA can be used to study vascular changes in the brain. A review of the research exploring vascular parameters of the retina for the changes in the brain is presented. It is found that several researchers have been able to detect retinal vasculature changes in association to the changes in the brain. Finally, OCTA segmentation techniques present in the literature are reviewed demonstrating that the use of deep learning models for segmentation yields best results amongst the other techniques.

Chapter 3

Methodology

This chapter contains the detailed explanation of the methodology that has been used in this research. The subsequent sections discuss the image acquisition, preprocessing, segmentation, feature extraction techniques that has been used. The outline of the methodology used is presented below.

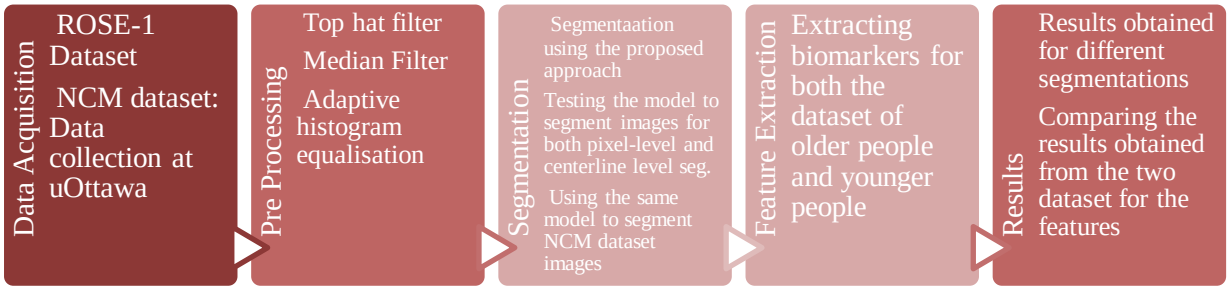

3.1 Data Acquisition

Even after recent surge in the studies based on OCTA images, there is a lack of publicly available published datasets with manual annotations. Several studies which have used the OCTA images to develop blood vessel segmentation techniques have used their own private dataset making it very difficult to validate and compare them. However, the success of the recently developed deep learning techniques can only be utilized if manual annotations (ground truth images) are present for the deep learning model to learn from. In 2020, Ma Y. et. al. [1] published a first publicly available OCTA dataset with manual annotations of the retinal microvasculature which has been used in this research. Furthermore, this dataset is particularly relevant for us as the subjects used in this dataset is the ageing population of two group, one group includes people who are diagnosed with Alzheimer's disease and the other is the control group. However, the authors of this dataset have not declared it yet, which image belongs to which group because they themselves are working

on it. Hence, for this study a combination of two datasets has been chosen, one is the ROSE-1 dataset [1] which contains images from ageing population and another dataset is the one which have been collected at the campus of University of Ottawa which includes images of younger population. Both the dataset will be discussed in detail in the following sections:

3.1.1 ROSE Dataset [1]

Retinal OCT-Angiography vessel Segmentation dataset was published in 2020 by Ma Y. et. al[1]. It consists of two datasets with images acquired from different devices. The subjects of both the datasets are very different from each other.

ROSE-1: It consists of a total of 117 OCTA scans (39 SVC images, 39 DVC images, 39 SVC+DVC images) obtained from subjects of two groups, there were 26 subjects of people diagnosed with Alzheimer's disease (AD) and 13 people of healthy control group. Hence, the dataset comprises of a total number of 39 subjects. The inclusion criteria for the dataset were that the participants must not be diagnosed with a known eye disease such as Glaucoma, AMD, very high myopia etc. Furthermore, they should not have a known systematic disease such as diabetes etc. The mean age of the participants was 68.4 ± 7.4 for the Alzheimer's group and 63 ± 10.2 for the controls. The OCTA device used to capture images was RTVue XR Avanti SD-OCT system (Optovue, USA) equipped with AngioVue software with a resolution of 304*304 pixels. The participants included in AD group were selected based on NINCDS-ARDA criteria. They did not go through any medical imaging process such as PET. The scan area used for these images were 3*3 mm^2 centered on fovea. SVC, DVC and SVC+ DVC were captured. Figure 6 shows three sample of images from ROSE-1 dataset of different qualities, these three images from the ROSE-1 dataset will be used throughout this thesis to observe the results at each step.

Figure 6: Examples of OCTA image from ROSE-1 dataset

As a part of this dataset, the authors also provided manual vessel annotations done by the clinical and imaging experts. Two types of annotations are provided for the ROSE-1 dataset:

1. Pixel-level annotations: These annotations were graded at pixel level by image experts for both SVC and SVC+DVC images as shown in Figure 7. This technique provides manually segmented images for the thicker blood vessels.

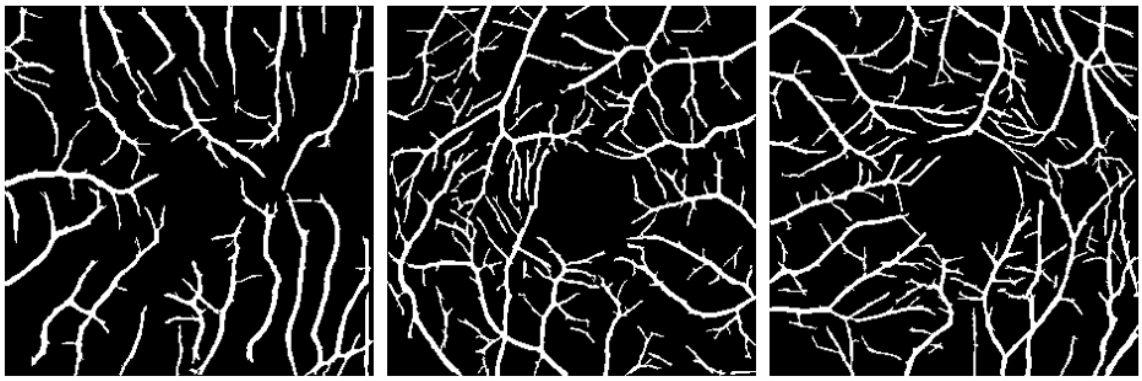

Figure 7: Examples of pixel-level annotations included in the ROSE-1 dataset

2. Centerline-level annotations: The capillaries in the SVC OCTA scan are small, so they were graded at the centerline as it was difficult to trace its diameter. However, centerline annotation includes thicker blood vessels as well. ImageJ software was used by the image experts to trace these annotations manually. SVC, DVC, and SVC+DVC are obtained using this method as shown in Figure 8.

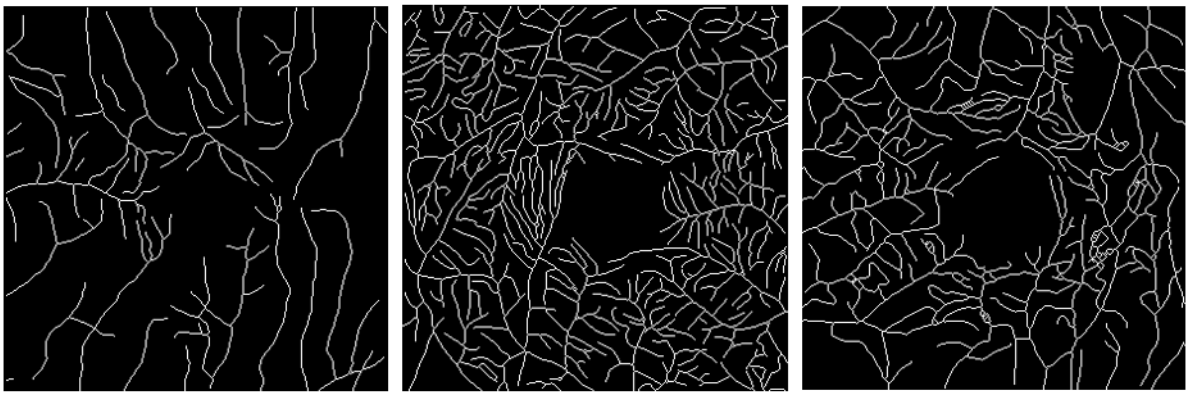

Figure 8: Examples of centerline-level annotations included in the ROSE-1 dataset

ROSE-2: It comprises of a 112 OCTA images collected from 112 eyes. The subjects of this dataset were people suffering from different macular disease. The device used to capture this dataset is the Heidelberg OCT2 system with Spectralis software. The SVC images were captured using this device with the scanning area of 3*3 mm^2 around the fovea. The OCTA images were reconstructed from 512*512 repeated scans with the inbuilt ART trucktrack system to reduce artefacts. For this dataset only the centerline-annotations are provided using a program written MATLAB by an experienced ophthalmologist.

Given the objective of this work involving the ageing population and the goal of finding vascular biomarkers associated to ageing or SVD and not any macular disease, only ROSE-1 dataset has been chosen to be included in this study along with the other dataset collected at university of Ottawa which is described in the next section.

3.1.2 NCM Dataset

As a part of this study, OCTA images of younger people have been collected to compare with the older people dataset to observe the changes in the retinal vasculature as a person ages. These images have been collected on the OCT system lab at University of Ottawa, Lees Campus. The OCT device at the university of Ottawa is the Heidelberg OCT2 system with Spectralis software.

Proper training was provided by an expert on how to take scans. The inclusion criterias for the participants were very similar to that in ROSE-1 dataset [1] which is a part of this study and are discussed as follows:

(i) The participants must not have any known macular disease such as glaucoma, AMD etc.

(ii) The participants must not be suffering from a known systematic disease such as Diabetes etc. All the participants were asked of these questions before their participation, no blood tests were done to confirm what they said.

(iii) Since this data collection is done for the younger population so the inclusion criteria for the age was that the participant must be of the age 18-50 years.

The collection of OCTA image required the participant to rest their chin on the OCTA machine and look into its camera at the blue light, while the person taking the scan calibrated their fovea with the white circle on the screen. Once it aligns, the camera was focused until a good quality image appeared on the screen. Subsequently, the image was captured when a good quality image appeared. These images were reconstructed by a 512*512 repeated A-scans with the Heidelberg automated real time (ART). All the images captured were SVC within 3*3 mm^2 area centered at the fovea. The images obtained were resized to a size of 304*304 to maintain the similar size throughout the dataset. A total of 8 people agreed to participate out of which 2 were sensitive to the blue light and hence no images were collected for them, two participants were losing focus and blinking a lot and hence due to very poor quality the OCT machine was unable to capture images for them. So in the end, OCTA images of 4 people were collected for both the eyes (total of 8 images), after removing the images with very poor quality as shown in Figure 9(A), the remaining images of younger population that were used in study was 5 (three images were discarded), a sample of which is shown in the Figure 9(B).

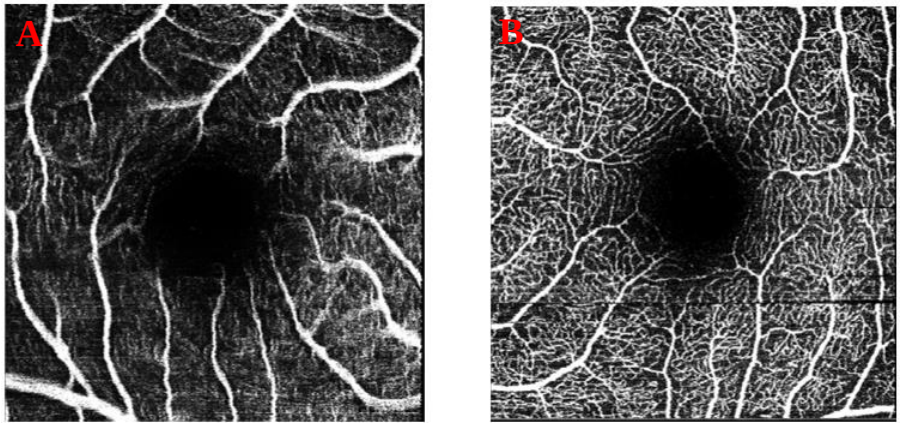

Figure 9: OCTA image captured in the lab of (A) poor quality and rejected (B) better quality and was accepted

3.2 Preprocessing

The preprocessing is an important image enhancement step used to suppress the unwanted distortions and noise while enhancing the features important for the further processing. Figure 10 shows the original images as in ROSE-1 dataset, Figure 11 shows the original NCM images. These images will be used as a reference for the image processing steps discussed in the sections below.

Figure 10: Original Images from ROSE-1 dataset of the examples used in this report

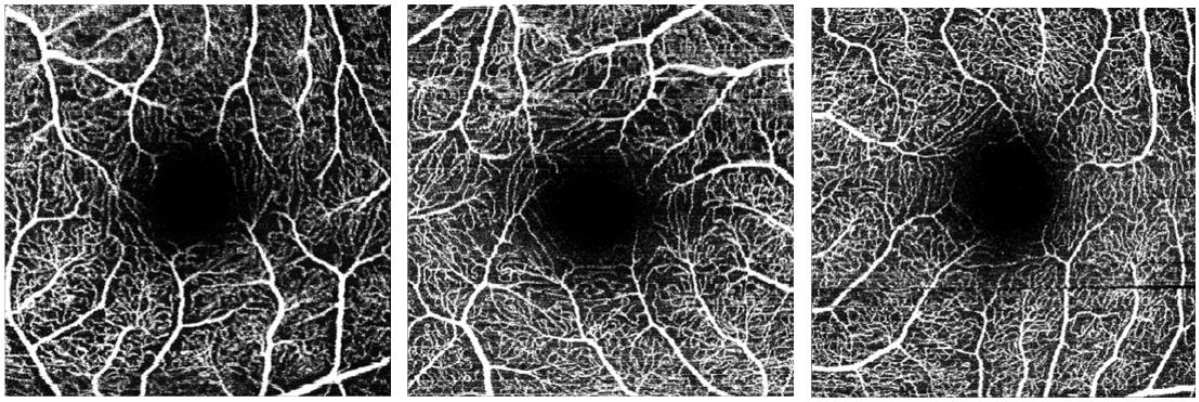

Figure 11: Original images from NCM dataset

3.2.1 Top hat Filter

It is a morphological operator which calculates the morphological opening of the image followed by subtracting the resulting image with the original one as shown in equation 1. The morphological opening refers to erosion followed by dilation. It is used to enhance the bright object over the black background. A Structuring element is used to perform the morphological opening, a matrix which is used to define the neighborhood for each pixel to process the image.

$$I_{TH} = I_G - (I_G)\ o\ e \quad (1)$$

Where, I_{TH} is the image transformed after using top hat filter, e is the structuring element used to perform the opening operator o.

The structuring element used in this study is a 6*6 square. The use of top hat filter as a preprocessing step to extract the blood vessels have been proven as a great success [65]. The use of this filter is to enhance the linear contrast and reduce the noise. Figure 12 shows three images from the ROSE-1 dataset after using the top hat filter. The images of ROSE-1 dataset went through this pre-processing only while performing pixel-level segmentation. However, the NCM images did not go through this pre-processing step as the contrast in the NCM images was already good.

Figure 12: Images from ROSE-1 dataset after performing Top hat filter operation

3.2.2 Median Filter

It is a non-linear filter which is used to remove spike noise, which looks like artificially bright pixels, while preserving the edges. This filter computes the median value of the pixels over a given window and assign that value to the pixel. The window size used in this study is 3*3. The Figure 13 shows the results obtained after median filtering the images from ROSE-1 dataset, Figure 14 shows a sample of images after performing median filtering over NCM images. Please note that this is the only pre-processing step performed over the NCM images.

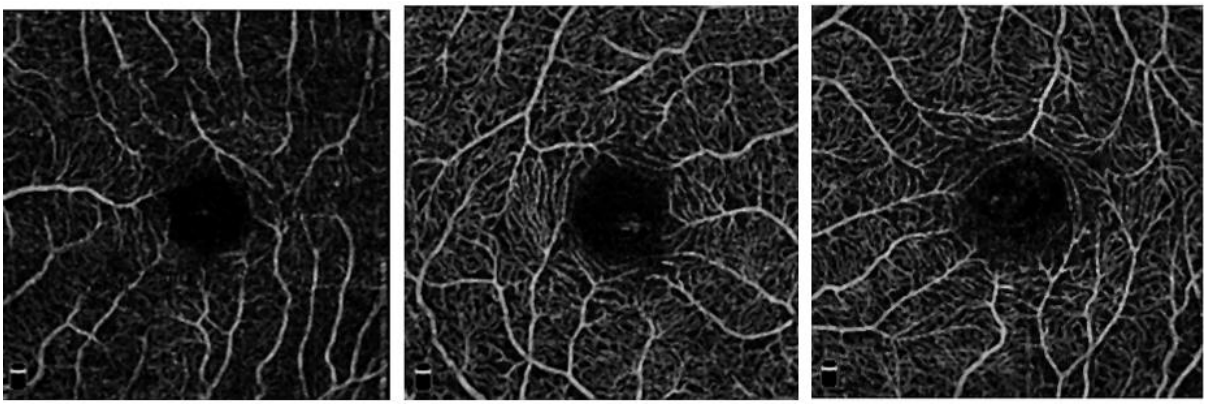

Figure 13: Images from ROSE-1 dataset after median filtering

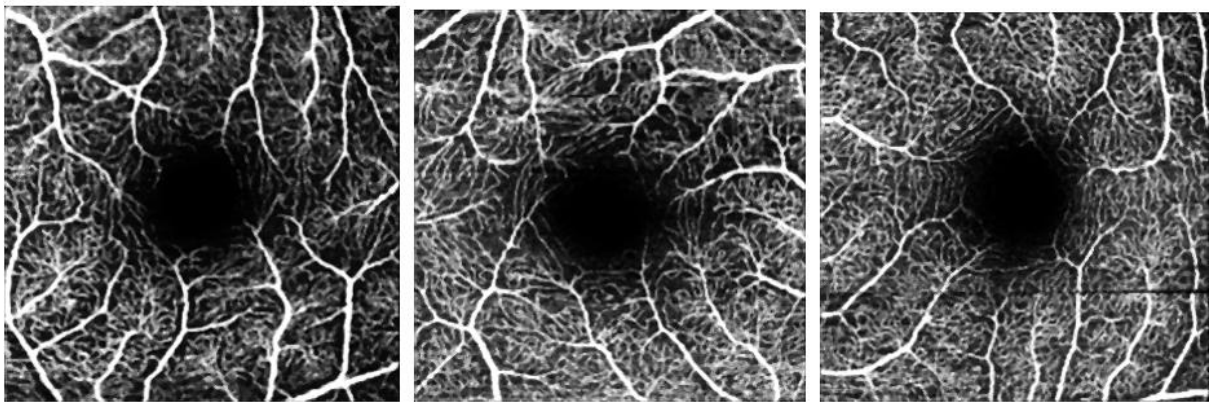

Figure 14: NCM images after median filtering

3.2.3 Adaptive Histogram Equalization

The local contrast of the image is improved by using Contrast limited adaptive histogram equalization (CLAHE) technique. After median filtering the image to reduce the noise, the contrast of some of the blood vessel decreased and hence to improve that without enhancing the noise, CLAHE has been used over the above obtained image. In CLAHE, the image is divided into smaller tiles, the histogram for each region is calculated and the clipping is performed at a fixed value. The clipped value is then redistributed over the entire histogram. The resulting images are shown in Figure 15. Please Note that, for centerline segmentation this is the only preprocessing step performed.

Figure 15: Images from ROSE-1 dataset after performing Adaptive histogram Equalization

To summarize, top hat filter, median filter and adaptive histogram equalization were used as preprocessing steps for pixel-level segmentation of ROSE-1 dataset. Adaptive histogram equalization was used as a preprocessing step for centerline-level segmentation of ROSE-1 dataset. Median filtering was used as a preprocessing step for NCM images

3.3 Segmentation:

In the recent years, many deep learning neural network have outperformed the state-of-the-art techniques in image segmentation especially in the biomedical image processing, where the accuracy achieved by using these methods is comparable to that of a radiologist. The use of deep learning techniques for the segmentation of various region of interest (ROI) in biomedical images is very popular such as tumor, pancreas, lungs etc. However, since OCTA is an emerging imaging modality, there is a need for an automated vessel segmentation technique. In this study, a novel blood vessel segmentation approach based on Attention UNet model is presented which is inspired by the model presented in the paper by Ma Y. et. al. [1] to perform pixel-level and centerline-level segmentation separately and then combine them. This approach is however simplified as compared to the model presented by Ma Y. et al. [1] where ResNetSt block with split attenuation [66] was used in the encoder-decoder stages for pixel-level and centerline segmentation and a fine stage was introduced where the resulting images pass through another layer of convolutional networks. The convolutional neural network typically requires a large dataset which is usually never available in medical image processing. However, with the development of UNet [67], an extension of fully convolutional neural network for the biomedical image segmentation, having a large dataset is not necessary for accurate segmentation. Subsequently, several variations of biomedical UNet architecture evolved, one of which is the Attention UNet architecture which has been used in this study.

3.3.1 Attention UNet Architecture

In 2018, Oktay et. al.[68] proposed the model of using attention gate (AG) for the medical image segmentation which learns to focus on different shapes and sizes of the structures in the region of interest. The model trained using the AG focuses on the necessary features in the foreground while suppressing the unwanted features of the background. The authors then integrated the attention gates in a well-known model used for biomedical image processing known as UNet and called the complete architecture as Attention UNet as shown in Figure 16.

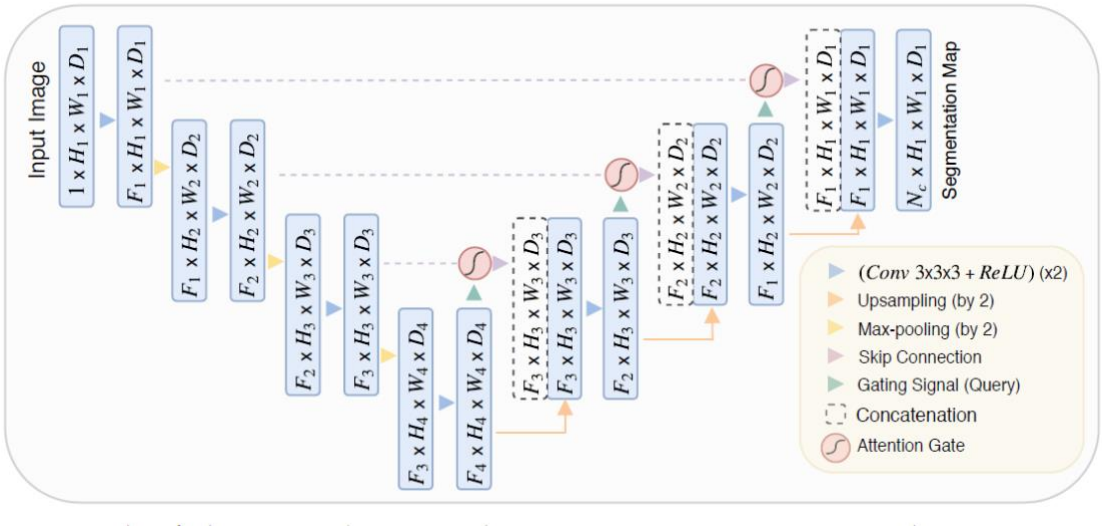

Figure 16: Attention UNet architecture as proposed in [68]

The architecture is similar to the one in UNet. The encoding part contains the filtered input image which is down sampled at each step by a factor of two, such that the $H_4 = H_1/8$. Subsequently, the resulting image is up sampled in the decoding stage by a factor of two. The features propagated through the skip connection are filtered by the Attention Gates (AGs) first.

Attention gates: The semantic contextual information in an image is obtained by down sampling the feature map grid in a convolutional neural network. However, the accuracy is decreased by the false positives obtained from small objects with greater scale variability. The accuracy is however increased by integrating attention gates in the convolutional neural network

model. This eliminates the need to train multiple models as done earlier and doesn't require large number of extra model parameter. The attention gate (as shown in Figure 17) reduces the feature response of the background without cropping the ROI.

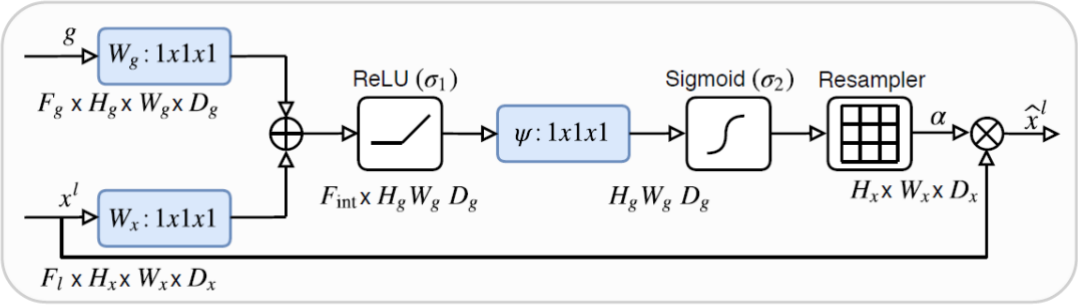

Figure 17: Attention gate model [68]

As shown in Figure 17, the two inputs to the attention gate includes a gating signal (g_i) which is obtained by up-sampled layer after it has been passed through the convolutional, batch normalization and ReLU layers. The other input is the input feature map (x^l) which is obtained through the skip connection (As shown in figure 16).

The gating signal (g_i) is used to determine the focus region of each pixel i. The output the AG is the multiplication of the attention coefficients $\alpha_{i,}$ and the input feature maps x^l as shown in Equation 2.

$$\hat{x}_{i,c}^l = x_{i,c}^l . \alpha_i^l \tag{2}$$

Where attention coefficients, $\alpha_i \in [0,1]$ identify the salient features in the image and reduce the feature response to keep the activation function relevant to the task. It is defined by the formula presented in Equation 3 and Equation 4.

$$q_{att}^l = \psi^T \left(\sigma_1\left(W_x^T x_i^l + W_g^T g_i + b_g\right)\right) + b_\psi \tag{3}$$

$$\alpha_i^l = \sigma_1(q_{att}^l(x_i^l, g_i; \Theta_{att})) \tag{4}$$

where, $\sigma_2(x_{i,c}) = \frac{1}{1+\exp(-x_{i,c})}$ is the sigmoid activation function which is chosen over the SoftMax activation function because its sequential use generates sparser activations at the output.

Hence, aiding better convergence of AG parameters. The gating signal takes the information obtained in the coarser stage and removes the irrelevant and noisy response in the skip connection. The output is then merged in the concatenation stage.

The next section presents the proposed segmentation approach used in this study to segment the SVC OCTA. The base model used for this approach is the Attention UNet.

3.3.2 Proposed Segmentation Approach:

As a part of this study, a novel segmentation approach has been proposed as shown in Figure 18 by using the Attention UNet architecture as the base model.

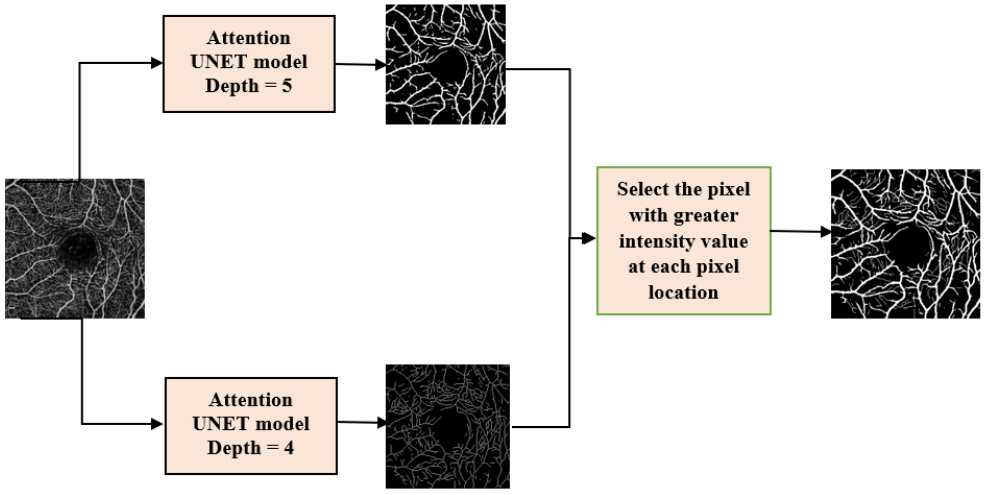

Figure 18: Proposed Segmentation approach

Since the annotated ground truth images had the pixel level annotations for the thicker blood vessel and center line annotation for the all the blood vessels, it was essential to segment them individually and then combine them in the end. An Attention UNet model of depths equal to 5 and 4 were used to perform pixel-level and centerline-level segmentation in SVC OCTA images. Batch normalization was employed in between convolutional and activation layer. A dropout layer of the rate equal to 0.2 was also added in between two convolutional layers. These two different depths Attention UNet models were trained for pixel-level and centerline-level segmentation.

The distribution of ROSE-1 images in training and testing images was included in the dataset. It was kept the same so that the results can be compared with the ones presented in the original paper [1]. The loss function used to train the model is the IoU (Intersection over Union) loss function. The IoU loss function is defined as the negative of the IoU coefficient (as given in Equation 5) which is also known as the Jaccard coefficient as presented in Equation 6.

$$IoU\ coefficient = \frac{Area\ of\ Overlap}{Area\ of\ Union} \tag{5}$$

$$IoU\ loss = -IoU\ coefficient \tag{6}$$

The IoU loss is the negative of IoU coefficient and it is used in this study because the higher the Jaccard coefficient (IoU coefficient) the better is the prediction. Since, the model tries to minimize the loss function, the negative sign added to the IoU coefficient will make sure that as IoU loss decreases, the IoU coefficient will increase.

Optimizers are algorithms responsible for changing the attributes such as weights and learning rate of the neural network to reduce the losses and provide accurate results. The optimization technique used in this study is the Adam optimizer [67] which takes the best features of other two optimizers, namely RMSprop and AdaGrad. The learning rate in Adam optimizer is adapted not only from the first momentum but also the second momentum of gradient i.e., uncentered variance. It has a faster running time, requires less tuning and is widely used in computer vision.

Once both the pixel-level and centerline-level segmentation of the test images were obtained by the respective trained models, the centerline-level segmented image was skeletonized to make it one pixel wise. Subsequently, the two segmented images were combined as shown in Figure 18. The final image is formed by choosing the pixel with higher intensity amongst both the segmented images at each location which is similar to performing pixel wise OR operation on the two segmented images as shown in Table 1.

Table 1: Pixelwise OR operation of the two segmented images

Pixel-level segmented image intensity value at location (i, j)	Centerline level segmented image intensity value at location (i, j)	Final segmented image intensity value at location (i, j)
0	0	**0**
0	1	**1**
1	0	**1**
1	1	**1**

3.4 Feature Extraction

Chapter 2 provides a survey of the most used vascular parameters utilized to study the decline in the cognitive ability of a person which may be because of diseases like CSVD, Alzheimer's etc. This section expands on the definitions of the vascular perimeters used in this study to compare the scans of the older individuals and younger individuals. The parameters used in this study are defined as follows:

1. Vascular Density: This is the most used vessel parameter in the literature while studying the cognitive decline of the brain [10]. It is calculated from a binarized segmented image as shown in Figure 19(B) and is defined as the total area of the flow divided by total area as shown in the Equation 7 [69]. This is a physiological parameter which considers both vessel length and diameter. Several studies have linked the decrease in Vessel density with decrease in cognitive decline [28][29], while a few have seen no difference between the two groups [33][34]f.

$$Vascular\ Density = \frac{Total\ vessel\ area}{Total\ area} \tag{7}$$

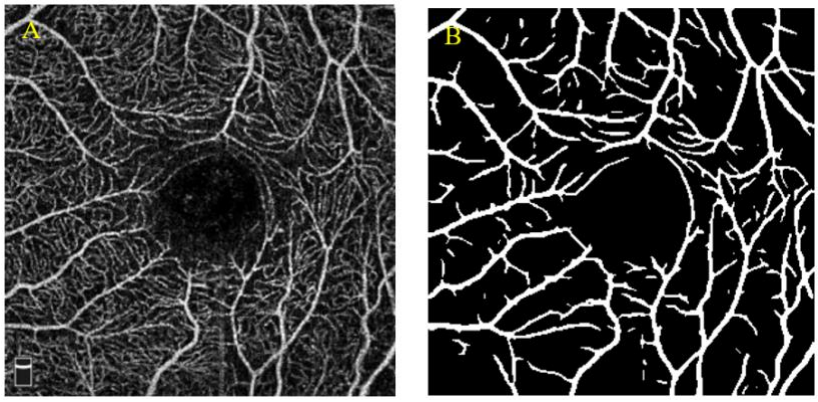

Figure 19: (A) Original image (B) Segmented image

2. Vessel Length Density: The ratio of the vessel length calculated after the skeletonization of the blood vessels as shown in Figure 20(B) and the total area of the image is known as the vessel length density (VLD)[69] [37] as shown in the Equation 8. Few studies [10] have used this parameter as a biomarker for cognitive health.

$$Vessel\ Length\ Density = \frac{\sum_{i=1,j=1}^{n} S(i,j)}{\sum_{i=1,j=1}^{n} I(i,j)} \quad (8)$$

Where S is total number of white pixels in a skeletonized image, and I is the total number of pixels in the image.

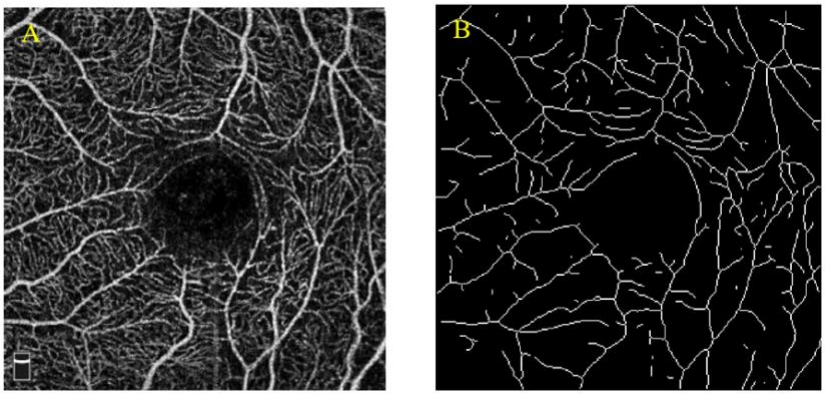

Figure 20: (A) Original image (B) Skeletonized image

3. Vessel Perimeter Index: It is calculated on the thicker blood vessels of the OCTA scans. This parameter is a good marker of tracking the changes in the vessel length of the OCTA image. The perimeter of the thicker blood vessel as shown in Figure 21(B) is calculated first and the Vessel perimeter Index is defined by Equation 9 [37].

$$Vessel\ Perimeter\ Index = \frac{\sum_{i=1,j=1}^{n} P(i,j)}{\sum_{i=1,j=1}^{n} I(i,j)} \tag{9}$$

Where, P is the total number of pixels in the perimeter of the vessel, and I is the total image area.

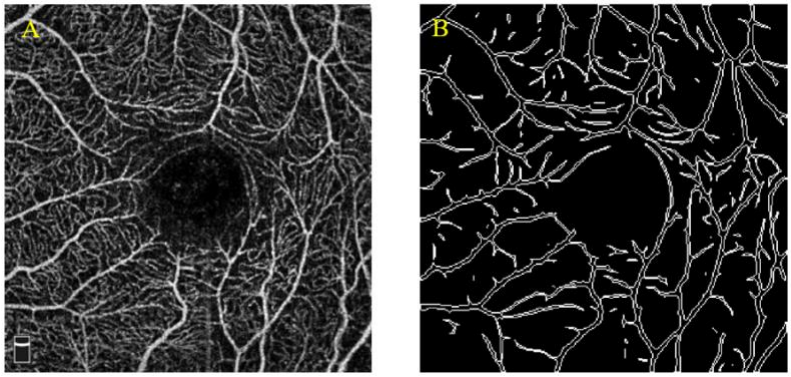

Figure 21: (A) Original Image (B) Perimeter of the segmented image

4. Mean Diameter of Blood Vessel: Any change in the blood flow will change the vasculature of the of the vessels, this can be tracked by the Mean diameter of the blood vessel. Large blood vessels are used to take this measure. It is defined [37] as the ratio of the vessel area and the vessel length as shown in the Equation 10. Vessel length is calculated after performing skeletonization of the blood vessels.

$$Mean\ vessel\ width = \frac{\sum_{i=1,j=1}^{n} B(i,j)}{\sum_{i=1,j=1}^{n} S(i,j)} \tag{10}$$

Where, B is the total number of white pixels in the segmented blood vessels as shown in Figure 22(A) and S is the total number of white pixels in the skeletonized image as shown in Figure 22(B).

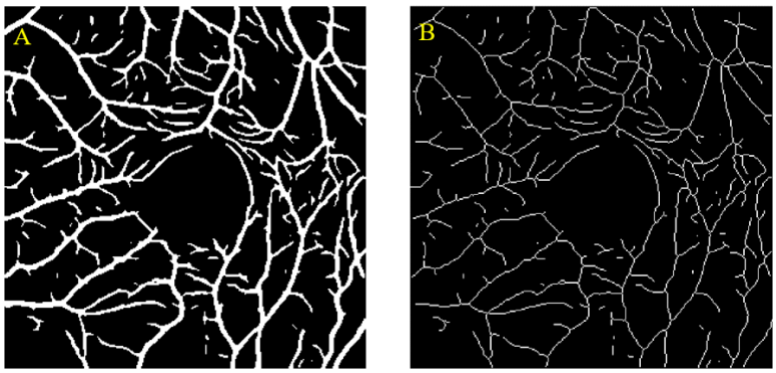

Figure 22: (A) Segmented image (B) Skeletonized image

3.5 Conclusion

This chapter provided the details of the methodology used. The dataset used for this study was defined. Subsequently, preprocessing steps for each segmentation was mentioned followed by the proposed segmentation approach. The details of the segmentation including the depth of the mode, optimizer and loss function was also discussed in detail. Finally, the features that were extracted as a part of this study were presented in detail. The next chapter comprises of the experimental details of this study and the results that were obtained.

Chapter 4

Results and Discussion

This chapter covers the results obtained after the segmentation of SVC OCTA scans using the proposed approach. Since, one of the objectives of this research was to study the changes in the vascular parameters of the OCTA scans amongst the older and younger individuals, this chapter also presents the features extracted (as discussed in section 3.4) from both the ROSE-1 dataset and NCM images. A comparison of all the features have also been presented for both the groups.

4.1 Experiment

The ROSE-1 dataset and the NCM images were first pre-processed using the techniques presented in Chapter 3. The ROSE-1 dataset was then divided into two parts (division was provided with the dataset). Out of 39 images, 30 were used for training purpose and 9 were used for testing purpose. The same pixel-level trained model was also used to segment images in the NCM dataset. The 30 images of the ROSE-1 dataset were used to train the Attention UNet model separately for both pixel-level and center-line blood vessel segmentation.

While training the neural network, forward and backward propagation is performed using the optimizer to update the weights. 1 epoch is when the complete dataset has passed through the network once (both forward and backward pass). In this study, the model is trained for 500 epochs for both the pixel-level and centerline-level segmentation. Validation split while training was 0.1, which means that at each epoch 90% of the training images were being used as a training set and the 10% were being used for validation, while the model was being trained. Adam optimization was used with an initial learning rate of 0.001 and an overwatch to stop the process if the validation loss does not improve for three epochs was used (also known as early stopping). The loss function used is the IoU loss function as defined in the Section 3.3.

As mentioned in the proposed segmentation approach in Chapter 3, two Attention UNet models with different depths were used to train for pixel-level and centerline-level segmentation with trainable parameters equal to 2,337,607 and 580,934 respectively. These trainable parameters are calculated as the sum of weights and biases of each layer. During training, the optimizer learns to optimize the weights and biases of the neural network. Hence, these are also known as tunable parameters. Once the models were trained, 9 testing images from the ROSE-1 dataset were used to test the model and segment the pixel-level and centerline-level images. Subsequently, both the segmented images were combined by performing pixelwise OR operation over the two images. Since, the evaluation metrics obtained for the defined segmentation approach were very high for pixel level segmentation, the trained pixel-level Attention UNet model was also used to segment the NCM dataset images. Finally, the features discussed in Section 3.4 were extracted and compared on the pixel-level segmentation for both ROSE-1 dataset and NCM images. The methodology discussed was implemented on the MATLAB R2020b and Google Colab.

4.2 Evaluation Metrics

The evaluation metrics are used to assess the performance of the proposed segmentation approach. All the metrics used in this study have different advantages and are essential to assess the results as well as the performance of segmentation model. Some of the metrics used in this study are to provide accurate estimate of the performance in the presence of class imbalance. These metrics are calculated in comparison to the manually segmented ground truths provided with the dataset.

True positive is when the pixel in the ground truth image and segmented image is a white pixel, true negative is when the pixel in both the ground truth and segmented image is a black pixel, false positive is when the pixel in the ground truth image is black whereas in the segmented image is white, false negative is when the pixel in the ground truth image is white and the segmented image is black. Considering TP represents True Positive, TN is True Negative, FP is False Positive, FN

is False Negative, TPR is the True Positive Rate, TNR is a True Negative Rate the evaluation metrics are defined as follows:

- Accuracy: Pixel accuracy is the most used metric to assess the performance of a segmentation. It is the percentage of the pixels that have been segmented correctly. Black pixels have been segmented as black pixels and vice versa, it is defined as given in Equation 11.

$$Accuracy = \frac{TP + TN}{TP + TN + FP + FN} \tag{11}$$

- Balance Accuracy (BAC): BAC is a measure of how well the classification has been done amongst the two classes (blood vessel and background), it is defined by Equation 12. This metric is especially used when there is a class imbalance, which means that the occurrence of one class dominates over the other. Since the images used in this study have a class imbalance, meaning there are more black pixels(background) as compared to the white pixels (blood vessels), this measure will balance that dominance and will give a fair indication of how well the segmentation has been performed.

$$BAC = \frac{TPR + TNR}{2} \tag{12}$$

Where, $TPR = \frac{TP}{(TP+FN)}$ and $TNR = \frac{TN}{(FP+TN)}$

- Dice Coefficient (DICE): Also known as F1 score, it is defined by the division of the area of overlap and total number of pixels of both the images (segmented and ground truth), as given by the Equation 13. It measures the similarity between two images/data (segmented and ground truth). It is used frequently to validate the image segmentation algorithms based on deep learning.

$$DICE = \frac{2 * TP}{2 * TP + FP + FN} \tag{13}$$

- Jaccard Coefficient (JAC): It is also known as Intersection over Union (IoU) and is defined by the area of overlap in between the segmented image and the ground truth divided by the area of union between the two images. The higher the value of Jaccard coefficient is, the greater is the overlap. The numerical formula for Jaccard coefficient is given in Equation 14.

$$JAC = \frac{TP}{TP + FP + FN} \tag{14}$$

- Kappa Score: It measures the degree of agreement in between the true value and predicted value and is defined by the Equation 15. It is used as a metric to evaluate segmentation algorithm's performance.

$$Kappa\ score = \frac{Accuracy - pe}{1 - pe} \tag{15}$$

$$where \quad pe = \frac{(TP + FN)(TP + FP)}{(TP + TN + FP + FN)^2} \tag{16}$$

- G-mean score: It considers both the majority and minority class and therefore determines the balance between the classifiers, it is given by the formula stated in Equation 17. It's an important measure which avoids the overfitting of the negative class (black pixels) and underfitting of the positive class (white pixels).

$$Gmean\ Score = \sqrt{sensitivity * specificity} \tag{17}$$

$$where, sensitivity = \frac{TP}{TP+FN} \text{ and } specificity = \frac{TN}{TN+FP} \tag{18}$$

The final centerline-level segmentation image is single pixel wide. Hence, as per the evaluation method for one-pixel wide curve, a tolerance region of three-pixel around the manually traced ground truth is considered for calculating true positive [1] [70]. This is done because the

centerline ground truth images were segmented manually at the center, and the centerline segmentation performed by the Attention UNet might be slightly shifted.

4.3 Segmentation Results

The metrics described above were used to evaluate the segmentation of test images on the SVC scans of ROSE-1 dataset, with respect to the ground truth images provided with the dataset. For NCM images, the segmented images are overlapped over the original image to validate the segmentation results.

4.3.1 ROSE-1 SVC Dataset

The results of SVC ROSE-1 dataset have three sections, the first section presents the results obtained by segmenting the pixel level segmentation (thicker blood vessels). The second section presents results obtained by segmenting the centerline-level segmentation (thinner blood vessels), whereas the third section discusses the results obtained after combining the two segmented images. Please note that, the ROSE-1 dataset includes ground truth segmented images for pixel-level segmentation, centerline-level segmentation, and the combination of the two. Lastly, a comparison of the results obtained by proposed approach is done with other deep learning techniques.

4.3.1.1 Pixel Level Segmentation Results:

The segmented images of thicker blood vessels with their respective ground truths and original images have been shown in Figure 23 for comparison. The results displayed are for images with different qualities, in some images, the presence of the artifacts is higher as compared to the others. By observing visually, it is evident that for each image, the Attention UNet model performed well. This has also been verified by analyzing the evaluation metrics presented in Table 2 for each test image and Table 3 for the average evaluation metrics. The segmentation of the thicker blood vessels in the OCTA images has been done with a very high average accuracy of 0.94981. All other evaluation metrics are also very high for these segmented images. The average dice coefficient

which is a measure of similarity between the segmented image and the ground truth came out to be 0.82815. The average Jaccard coefficient is 0.70698 which reflects greater overlap in between the segmented image and the ground truth, The average balance accuracy is also very high and is equal to 0.91894. All these evaluation metrics indicates towards the success of the Attention UNet model for the segmentation of the thicker blood vessels.

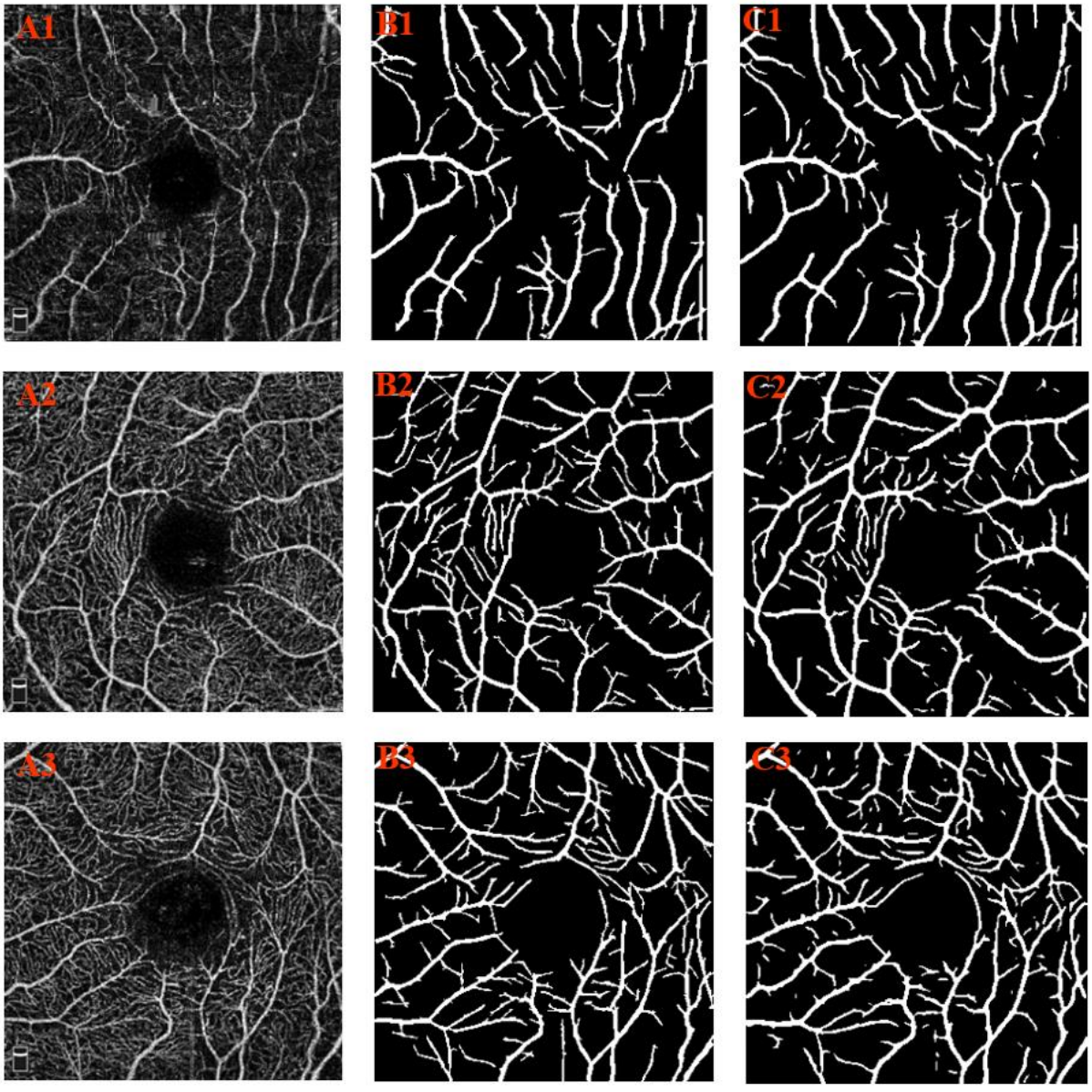

Figure 23:For pixel-level segmentation (A1-A3) Original images (B1-B3) Ground Truths (C1-C3) Segmented Images

Table 2: Pixel-level segmentation results of the ROSE-1 dataset for the 9 test images

Image Number	Accuracy	Dice Coefficient	Jaccard Coefficient	Kappa score	Balance accuracy
1	0.96292	0.85874	0.75246	0.83740	0.91977
2	0.95213	0.80923	0.67958	0.78198	0.91299
3	0.94985	0.83582	0.71795	0.80656	0.94025
4	0.94102	0.82231	0.69824	0.78697	0.90143
5	0.95942	0.83422	0.71559	0.81118	0.92653
6	0.94527	0.82200	0.69780	0.79004	0.93146
7	0.94622	0.82670	0.70459	0.79524	0.93422
8	0.93983	0.80680	0.67616	0.77116	0.88757
9	0.95166	0.83755	0.72050	0.80919	0.91621

Table 3: Average of the evaluation metrics for pixel-level segmentation of the ROSE-1 dataset

Average Accuracy	Average Dice-coefficient	Average Jaccard Coefficient	Average Kappa score	Average Balance accuracy
0.94981	0.82815	0.70698	0.79886	0.91894

4.3.1.2 Centerline-level Segmentation Results:

The segmentation of the thinner blood vessels has been done using the Attention UNet model with a depth equal to 4, followed by skeletonization to make it one pixel wide. A few examples of the original image manually traced ground truth image and segmented image have been presented in the Figure 24. The centerline-level segmentation is a challenging task as the background blood vessels are the most affected by the presence of artifacts. If the ground truth image as show in Figure 24(B1) of Figure 24(A1) is observed, it can be seen that most of the capillaries behind the thicker blood vessels have not been traced manually. However, for an OCTA image which are less affected by the artifacts as shown in Figure 24(A2 & A3), the manually segmented ground truth as shown in Figure 24(B2 & B3) have highlighted most of the capillaries as well. Therefore, it has

been observed that when the model learns from such varying training ground truth images, it is not able to segment thinner blood vessels in the spaces which are somewhat blurred due to artifacts. Figure 24 provides a visual comparison in between the original images (A1-A3), Ground truths (B1-B3) and their respective segmented images (C1- C3) for centerline-level segmentation.

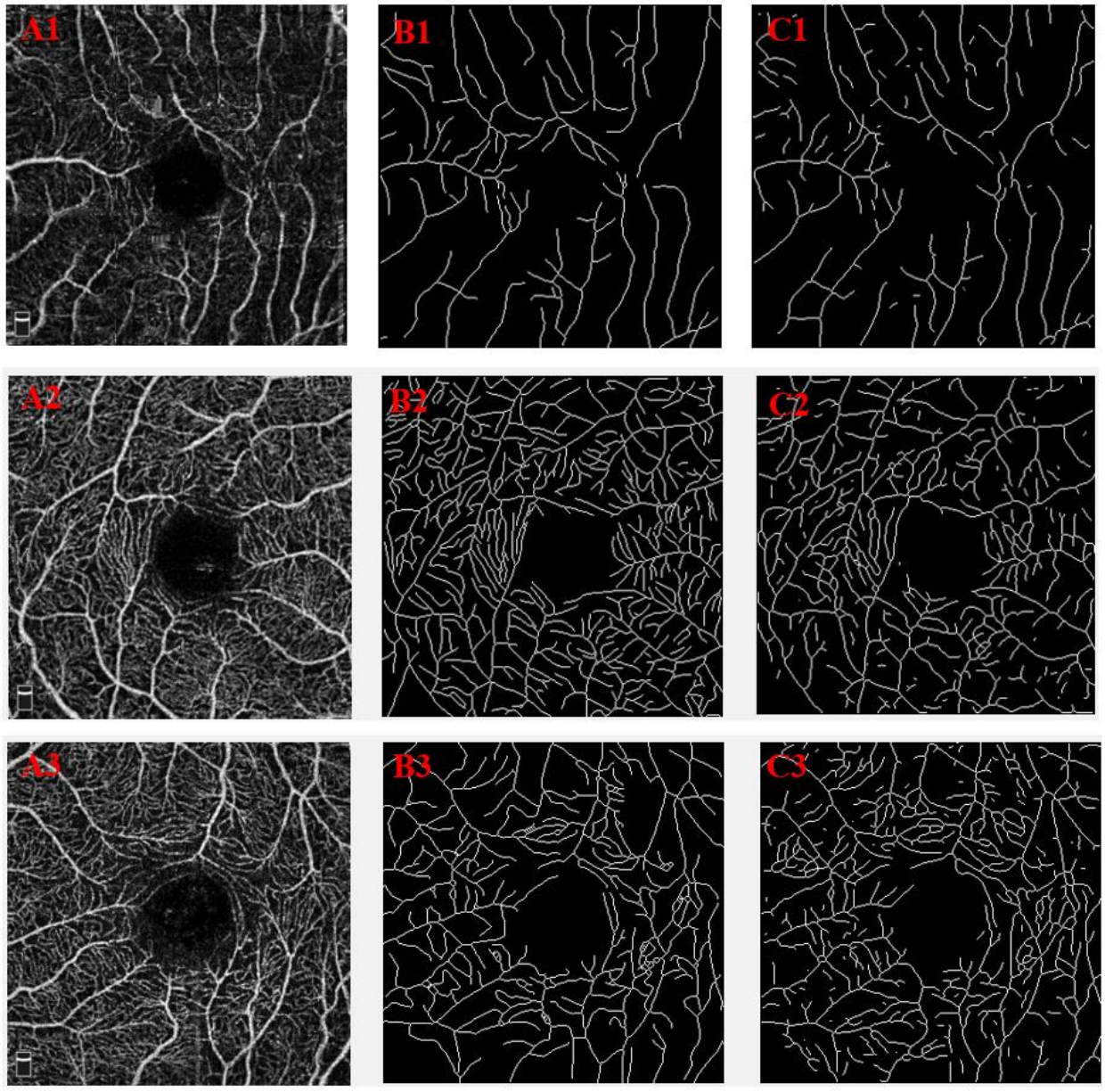

Figure 24: For centerline-level segmentation (A1-A3) Original images (B1-B3) Ground Truths (C1-C3) Segmented Images

The evaluation metrics are in synchronization with the visual observations as shown in Table 4 and Table 5. The accuracy of the segmentation is 0.92982, which is very high because of the class imbalance, hence average balance accuracy is also calculated and found to be 0.72282 which is good. The dice coefficient is 0.58919 and average Jaccard coefficient is 0.41925 which is a measure of overlap. Since, the ground truth is a centerline annotation which is one-pixel wide, low Jaccard coefficient is reasonable. The average kappa score value is also 0.55568.

Table 4: Results of the centerline-level segmentation for the 9 test images of the ROSE-1 dataset

Image Number	Accuracy	Dice-coefficient	Jaccard Coefficient	Kappa score	Balance accuracy
1	0. 96813	0. 65820	0. 49054	0. 64221	0. 77013
2	0. 94609	0. 54417	0. 37379	0. 52014	0. 69348
3	0.93917	0. 63833	0. 46879	0. 60734	0. 7504
4	0. 93393	0. 63466	0. 46483	0. 59928	0. 76434
5	0. 95982	0. 61498	0. 44402	0. 59524	0. 74125
6	0. 89022	0. 52942	0. 36001	0. 48045	0. 68180
7	0. 90664	0. 52608	0. 35692	0. 48497	0. 68103
8	0. 91737	0. 59953	0. 42809	0. 55797	0. 72490
9	0. 90700	0. 55731	0. 38630	0. 51351	0. 69825

Table 5: Average of the evaluation metrics for centerline-level segmentation of the ROSE-1 dataset

Average Accuracy	Average Dice-coefficient	Average Jaccard Coefficient	Average Kappa score	Average Balance accuracy
0.92982	0.58919	0.41925	0.55568	0. 72284

4.3.1.3 **Fully Segmented SVC Image:**

Once both the pixel-level and centerline-level segmentation was done separately, examples shown in Figure 23 and Figure 24. According to the proposed approach, they were merged into a final segmented SVC image by comparing the intensities at each pixel location and choosing the highest intensity amongst the two, similar to performing pixelwise OR operation on the two images (as discussed in Table 1). Figure 25 shows the original images (A1-A3), ground truths (B1-B3) and the final segmented images (C1-C3) of the blood vessels obtained after performing segmentation according to the proposed approach. The images displayed are for various artifacts level. Visually, the proposed segmentation technique appears to be segmenting the SVC OCTA scan accurately with some finer blood vessels missing in areas with artifacts, which is lowering the evaluation metrics for the SVC image segmentation.

Table 6 and Table 7 shows the evaluation metrics obtained for the fully segmented images (Pixel-level + centerline segmentation). The segmentation approach of SVC OCTA scans gives high average accuracy of 0.91887, the dice coefficient is also almost more than 0.75 for every image with an average of 0.7853. The mean value of Jaccard coefficient is 0.64813, which indicates the overlap of Ground truth value and segmented image. The average kappa score of the segmented image 0.73541 and a high average balance accuracy of 0.85518. To alleviate the class imbalance G-mean score has also been calculated and is found to be 0.84739 which proves that this segmentation approach is very good for the segmentation of SVC OCTA scans.

Table 6: Evaluation metrics for fully segmented 9 SVC OCTA images from ROSE-1

Accuracy	Dice coefficient	Jaccard Coefficient	Kappa score	Balance accuracy	G-mean score
0.95806	0.85353	0.74449	0.82908	0.90649	0.90355
0.93217	0.77237	0.62916	0.73265	0.85134	0.84315
0.93074	0.81655	0.68998	0.77387	0.89063	0.88833
0.92507	0.81583	0.68895	0.76880	0.88420	0.88151
0.94667	0.80775	0.67750	0.77679	0.88850	0.88484
0.87758	0.72717	0.57130	0.64997	0.80031	0.78481
0.89477	0.74752	0.59683	0.68185	0.81963	0.80785
0.90268	0.76669	0.62165	0.70590	0.83149	0.82110
0.90204	0.76030	0.61330	0.69981	0.82401	0.81139

Table 7: Average of the evaluation metrics for fully segmented SVC OCTA scans

Average Accuracy	Average Dice-coefficient	Average Jaccard Coefficient	Average Kappa score	Average Balance accuracy	Average G-mean score
0.91887	0.78530	0.64813	0.73541	0.85518	0.84739

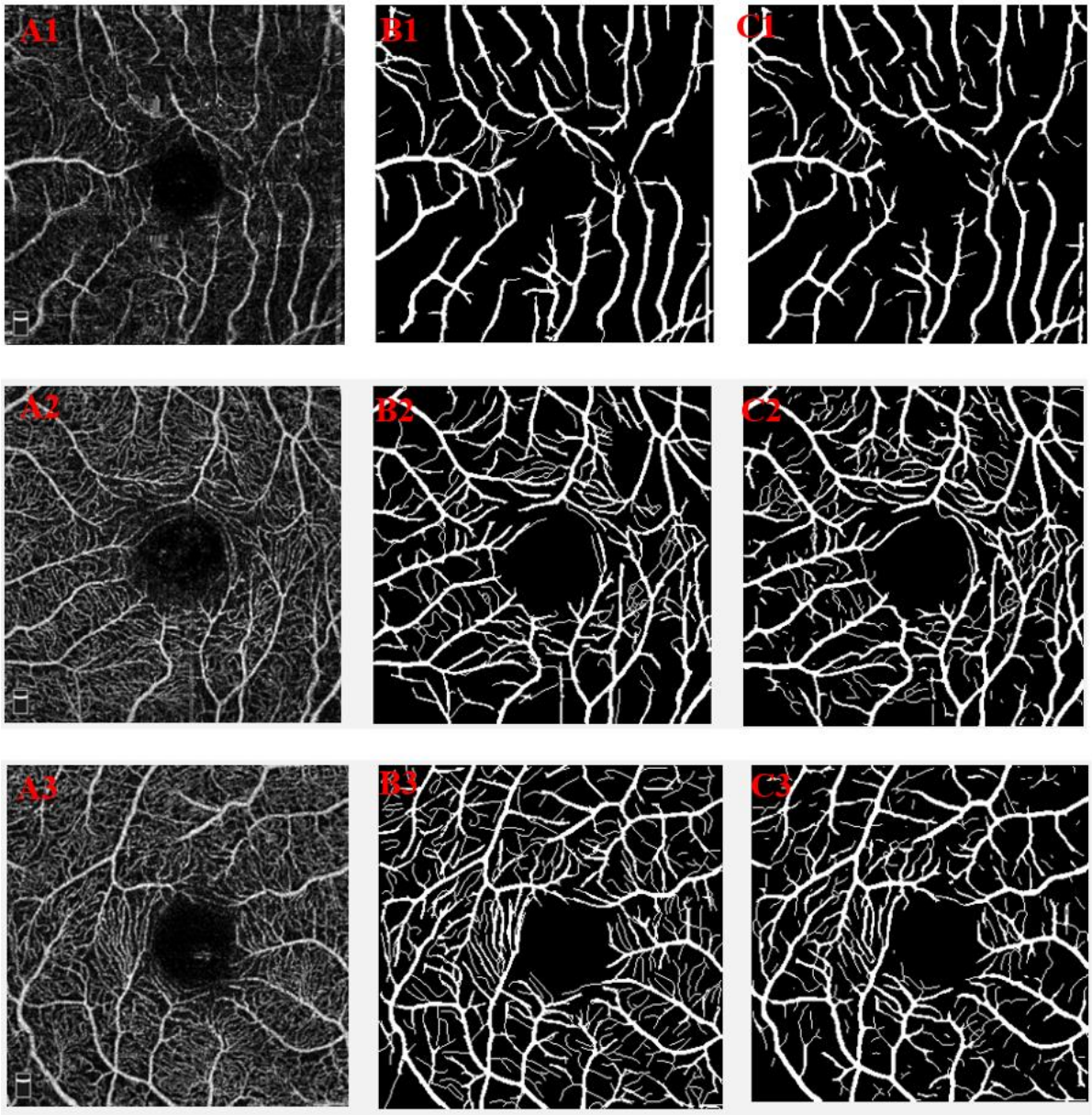

Figure 25:Fully segmented SVC image (A1-A3) Original images (B1-B3) Ground Truths (C1-C3) Segmented Images

4.3.1.4 **Comparison with other Segmentation Algorithms:**

The SVC results obtained from the proposed segmentation approach were compared with the results presented in the paper [1] for different segmentation methods. The results obtained are shown in Table 8. It can be seen that the results achieved by the presented segmentation approach outperforms all other segmentation methods in all the performance metrics. Ma Y. et al. [1]

mentioned that their segmentation model "OCTA Net" provides the best results amongst other deep learning methods, but the segmentation approach presented in this paper performs even better than the OCTA Net with a slight increase in the accuracy from 0.9182 to 0.91887, the G-mean score had an increase of 1.1% from 0.8361 to 0.84739. The kappa score increased by 1.5% from 0.7201 to 0.73541 and Dice coefficient increased by 1.56% from 0.7697 to 0.7853. Please note that, the training and testing images division were kept the same as presented by Ma Y. et al. [1], so that the comparison can be made.

Table 8: Comparison of fully segmented OCTA images using various deep learning techniques and the proposed approach

Methods	**Accuracy**	**G-mean**	**Kappa**	**Dice**
U-Net [1]	0.8955	0.8068	0.6476	0.7116
Res U-Net [1]	0.9098	0.8229	0.6911	0.7461
CE-Net [1]	0.9121	0.8256	0.6978	0.7511
DU Net [1]	0.9118	0.8249	0.6970	0.7505
CS-Net [1]	0.9152	0.8304	0.7093	0.7608
OCTA-Net [1]	0.9182	0.8361	0.7201	0.7697
Presented Segmentation Approach	**0.91887**	**0.84739**	**0.73541**	**0.7853**

4.3.2 NCM Images Segmentation:

Due to the absence of the ground truth images for the NCM images, the evaluation of the segmentation of thicker blood vessels of the NCM images is done by overlapping the segmented images over the original image and assessing it visually.

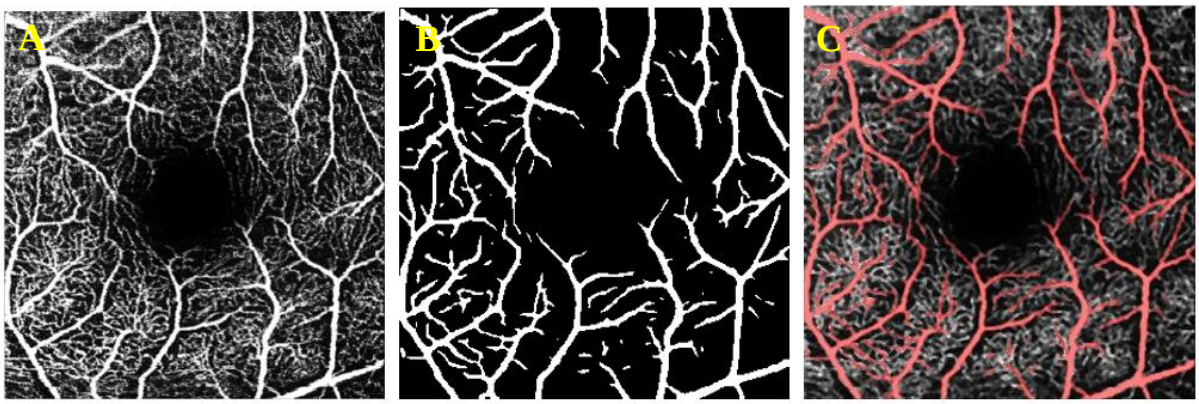

Figure 26: NCM image 1 - (A) Original image (B) Segmented image (C) Segmented image overlapped over original image

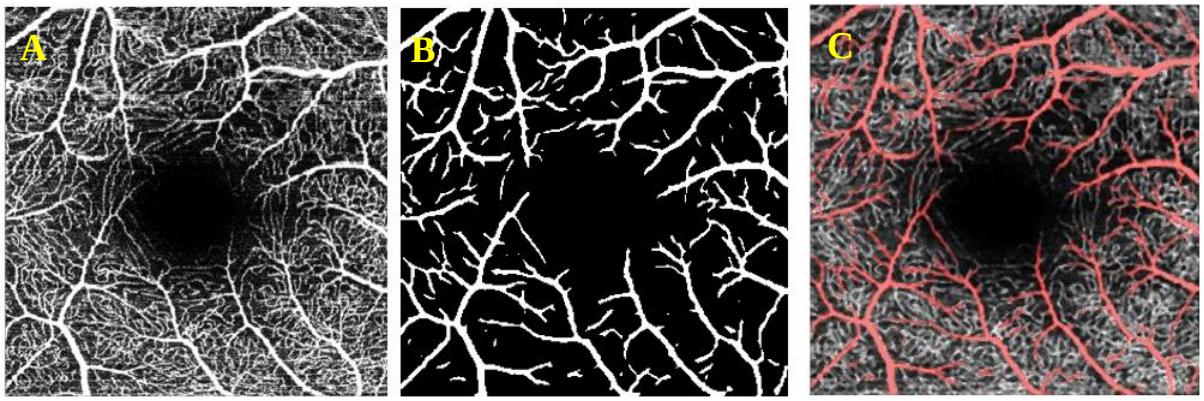

Figure 27: NCM Image 2 - (A) Original image (B) Segmented image (C) Segmented image overlapped over original image

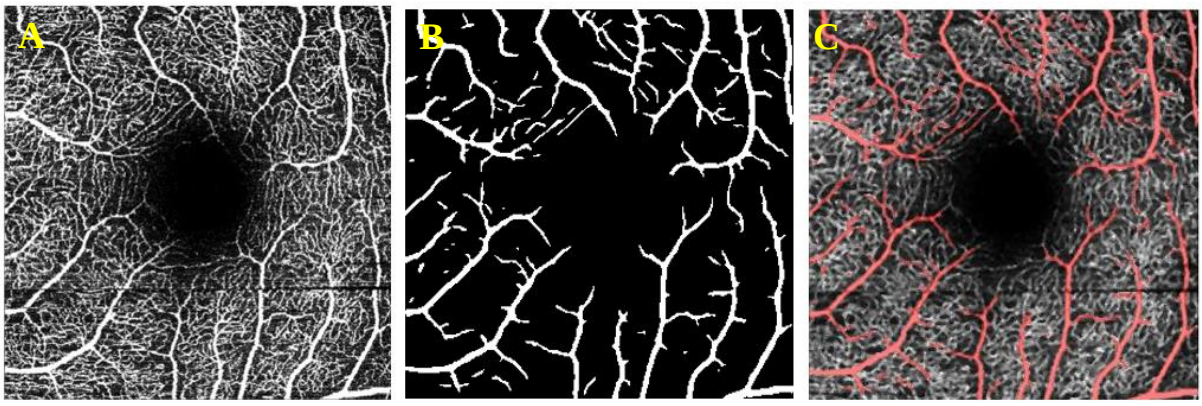

Figure 28: NCM image 3 - (A) Original image (B) Segmented image (C) Segmented image overlapped over original image

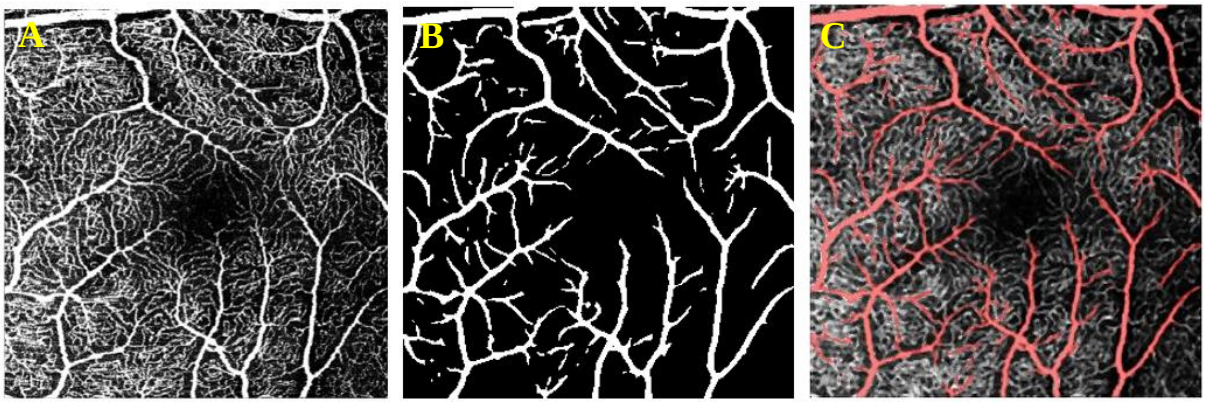

Figure 29: NCM image 3 - (A) Original image (B) Segmented image (C) Segmented image overlapped over original image

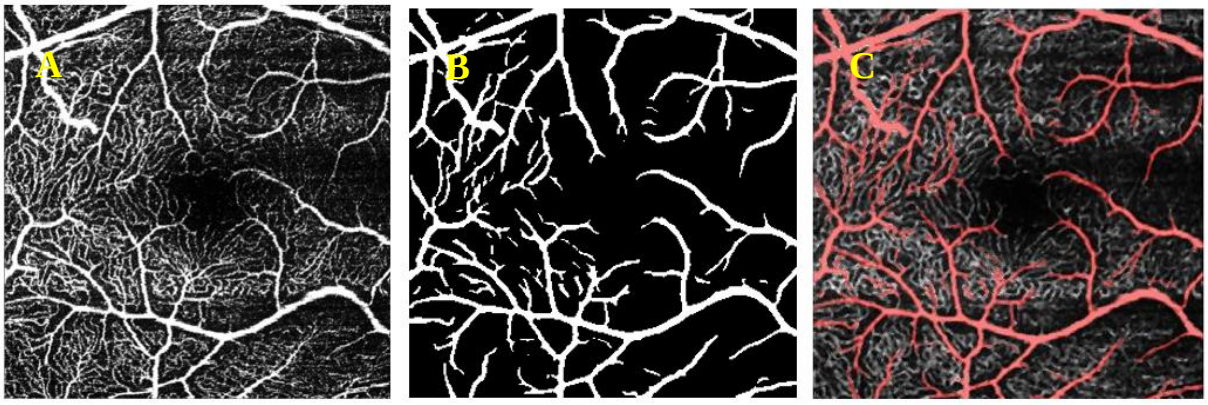

Figure 30: NCM image 4 - (A) Original image (B) Segmented image (C) Segmented image overlapped over original image

Figures 26 - 30 indicates good pixel level segmentation which involves segmenting the thicker blood vessels of NCM images using the trained Attention UNet model. It is observed that the finer details at the end of each blood vessel in the SVC OCTA scans of the NCM images are also preserved. By examining Figure 28 and Figure 30, it can be seen that the trained model performs well even in the presence of artifacts. Please note that, the images on which Attention UNet model was trained were captured from RTVue XR Avanti SD-OCT system machine (ROSE 1 dataset), while the NCM images have been captured from the Heidelberg OCTA system. In other words, the model was trained over ROSE-1 dataset and NCM images were segmented using the

same trained model. This shows that the Attention UNet model works greatly for the segmentation of thicker blood vessels even if OCTA images were captured from different systems.

4.4 Feature Extraction Results:

Once the thicker blood vessel of the SVC OCTA images were segmented for both the ROSE-1 dataset as well as NCM images, the features as mentioned in the Section 3.4 were extracted. Please note that ROSE-1 dataset contains the images of older individuals and NCM images were captured for young indiviuals. The next objective of this study was to extract the vascular features and compare it for both the older people and young individuals. Therefore, the extracted feature values are presented in Table 9 for ROSE-1 dataset and Table 10 for NCM images.

Table 9: Extracted feature values from the ROSE-1 dataset (Older individuals)

Vessel Density	**Vessel Length Density**	**Vessel PerimeterIndex**	**Mean Diameter of Blood vessel**
0.13165	0.035654	0.070561	3.6926
0.13312	0.037548	0.073277	3.5452
0.16776	0.046475	0.089974	3.6098
0.17002	0.050446	0.096866	3.3704
0.12924	0.035979	0.070053	3.5922
0.16896	0.045858	0.088307	3.6845
0.17052	0.047935	0.091672	3.5573
0.15670	0.045771	0.088156	3.4236
0.15373	0.042200	0.082951	3.6428
Average Values			
0.1535	0.04310	0.0835	3.5687

Table 10: Extracted features values from the NCM images (younger individuals)

Vessel Density	**Vessel Length Density**	**Vessel Perimeter Index**	**Mean Diameter of Blood vessel**
0.17552	0.043899	0.084931	3.9983
0.16646	0.045652	0.088296	3.6464
0.12684	0.035557	0.069901	3.5673
0.16249	0.042428	0.082507	3.8299
0.17548	0.044733	0.085407	3.9228
Average Values			
0.1614	0.0425	0.0822	3.7929

4.4.1 Statistical Analysis

A statistical analysis is performed to assess the statistical significance of difference for the measured metrics in both the populations (older and younger individuals) using T-tests. The T-tests is used in hypothesis testing to determine whether the measured metrics for the two groups are different for one another or not. A null hypothesis describes that there is no difference between the two groups. Alternate hypothesis is the opposite of null hypothesis i.e., the two groups are statistically different. This is decided based on p-value, which determines that how likely the data could have occurred under the null hypothesis. If the p-value calculated during the t-test is less than 0.05, it means that the result is statistically different which means the null hypothesis has been rejected. However, if the p-value is greater than 0.05, that means the null hypothesis has been accepted and the two groups are not statistically different for the given metrics.

The T-test used in this study is the Independent T-test because the two groups belong to two unrelated categories older and younger individuals. The analysis is performed for the all the measured metrics namely, vessel density, vessel length density, vessel perimeter index and mean

diameter of blood vessels using Table 9 and 10. The results demonstrated a significant decrease in the mean diameter of blood vessels in 9 samples of old adults (M = 3.5686, SD = 0.1103) as compared to 5 samples of young adult (M = 3.7929, SD = 0.1822), t(12) = 2.9034, p-value of 0.0132 indicating a significant age-related blood vessel thinning. There was no significant effect on the vessel density, t(12) = 0.7586, p-value of 0.1888 despite a slight decrease in mean value in older adults (M = 0.1535, SD = 0.0177), as compared to young adults (M = 0.1614, SD = 0.0201). There was no significant effect on vessel length density, t(12) = 0.2280, p-value of 0.8235 between the young adults (M = 0.0425, SD = 0.0040) and the old adults (M = 0.0431, SD = 0.0055). Finally, there was no significant effect on the vessel perimeter index, t(12) = 0.2617, p-value of 0.7980 between the old adults (M = 0.0835, SD = 0.0099)and young adults (M = 0.0822, SD = 0.0072).

4.5 Discussion

The results discussed in section 4.3 shows that the proposed approach works well for the segmentation of SVC OCTA images with a high average accuracy of 91.887%, balance accuracy of 85.518% and G-mean score of 84.739. A comparison of the results obtained has also been done with other deep learning approaches results presented by Ma Y. et al. [1]. It was found that the segmentation approach proposed in this study outperforms others in terms of all the evaluation metrics discussed. The pixel level segmentation trained Attention UNet model was also used to segment the thicker blood vessels of NCM images. The results were presented in the form of image overlay of the segmented image over original image. By visual analysis, it was concluded that the Attention UNet model works well for the NCM dataset which was captured with another OCTA device.

Finally, Section 3.5 presented the results of the next part of this research which was to study the vascular features of younger group and older group and compare the two. It was found that the mean vessel diameter of older people decreases when compared to younger people (p-value

< 0.05). The other evaluation metrics were not statistically different according to the statistical analysis performed (p-value > 0.05).

4.6 Conclusion

This chapter included the experimental results obtained during this research. It started with presenting the pixel-level segmentation results followed by the results of centerline-level segmentation. Subsequently, the results of the proposed segmentation approach used for segmenting SVC OCTA images are presented and compared with those presented by Ma Y. et al. [1]. The same trained pixel level segmentation Attention UNet model was used to segment the NCM images, and the visual analysis of the results were made. Finally, completing the last objective of this research the feature extraction of both the older and younger groups are performed and compared statistically.

Chapter 5

Conclusion

The thesis presented an analysis of the OCTA images and how they can be used as a window to an aging brain by analyzing the vascular components of eyes. This report covered everything from the acquisition of data at the University of Ottawa lab (young individuals) and using it along with a publicly available dataset ROSE-1 (older individuals) for the segmentation of SVC OCTA images employing the proposed novel segmentation approach. It also includes a comparison of the vascular features extracted for both the groups (older and younger individuals).

Chapter 1 presented the introduction to the problem and the motivation behind it. The high-level objective of this research was to collect OCTA images for younger individuals, perform the segmentation task accurately using deep learning technique and eventually using the segmented images to extract vascular features from the eyes and analyzing them for the two groups (older, and younger participants). Chapter 2 details the theoretical background of the subject and goes over related work that has been published. It starts with the description of the changes that occurs in the brain of an older individual due to cerebral small vessel disease (CSVD) leading to diseases like Alzheimer's and dementia. Subsequently, an overview of these changes that reflects in the eyes because of its embryological connection to the brain is presented. The work that has been done till date in the same field is discussed along with a discussion of various OCTA segmentation techniques present in the literature.

The main objective of this research was to develop an automated segmentation tool for OCTA images, because of the difficulties that are encountered during manual segmentation. Therefore, Chapter 3 comprised of the methodology used in this study starting with the data acquisition done at the University of Ottawa lab, these images were combined with the publicly available ROSE-1 dataset to form a dataset used for the analysis in this research from two groups:

older and younger. The ROSE-1 dataset contained images from older people including images from the control group as well as from people suffering with Alzheimer's disease. However, the authors have not revealed which image belong to which group. Hence, images were collected at the University of Ottawa lab of younger individuals. The chapter also presented the proposed novel segmentation approach used to segment the SVC OCTA images by performing pixel level segmentation and centerline-level segmentation separately using Attention UNet model and then combining them. It also described the vascular features from the literature that can be extracted and compared for both the groups to assess vascular changes due to aging and cognitive decline of the brain.

The results of the work done were discussed in chapter 4, where the Attention UNet model with a depth of 5 trained from the pixel level ground truth, segmented the thicker blood vessel in the SVC images in ROSE-1 dataset with very high mean accuracy of 94.981%, average dice coefficient of 82.815%, Jaccard coefficient of 70.698% indicating good overlap between the ground truth and the segmented images, kappa score of 79.886% and high balance accuracy of 91.894% which takes into account the class imbalance in the images. Another conclusion which was derived from this research was that Attention UNet deep learning model work really well for the segmentation of OCTA thicker blood vessels.

Subsequently, another Attention UNet model with the depth of 4 was trained for the centerline annotations for SVC ROSE-1 dataset. The segmentation was followed by skeletonization to make the result 1 pixel wide. The results demonstrated segmentation of all the blood vessels including the thinner blood vessel with good average accuracy of 92.982% and average balance accuracy of 72.284%, where true positive for the centerline segmentation was calculated with a three-pixel tolerance region. Rest of the evaluation metrics were acceptable too as the segmented image was a centerline segmentation which is one-pixel wide and therefore has higher chances of results not overlapping with ground truth. The average evaluation metrics for the dice coefficient,

Jaccard coefficient and kappa score were 58.919%, 41.925% and 55.568%. respectively. Next according to the proposed segmentation approach the two segmented images namely: pixel level segmentation and centerline segmentation were combined, and the resulting images were compared with the ground truth images provided with the dataset. It was found that the overall segmentation of SVC OCTA images was done with a high average accuracy for 91.887% and average balance accuracy of 85.518%, average G-mean score was also calculated as 84.739%, average dice coefficient equal to 78.53%, average Jaccard coefficient and kappa score equal to 64.813% and 73.541% respectively. A comparison was also made with the other deep learning techniques, and it was found that the images segmented through the proposed segmentation approach outperforms the others in every evaluation metrics. Since, the evaluation metrics for the pixel level segmentation of blood vessels was high, the same trained model was used to segment thicker blood vessels in the NCM images, which were evaluated visually by overlapping segmented image over original image. It was concluded that the Attention UNet model was able to perform pixel-level segmentation successfully.

Finally, chapter 4 discussed the last objective of this research which was to extract vascular features for the two groups and study them. For this, only the thicker blood vessel (pixel-level) segmentation was considered as the centerline-level segmentation was affected by the artifacts which was affecting its segmentation by a greater extent. Using the fully segmented image would have led to inaccurate results because of the absence of centerline segmented blood vessels in areas affected by the artifacts (as can be seen in Figure 25). Please note that, even the ground truth images did not have the annotations of capillaries affected by the artifacts. Further, as the ground annotations for the NCM images were not present, it was difficult to analyze the performance of the given segmentation algorithm for fully segmented NCM images. Hence, this research only focuses on studying the thicker blood vessels for vascular feature extraction from both the groups namely, ROSE-1 dataset for older individuals and NCM images for younger individuals. A

statistical analysis was performed to study the statistical significance of difference for the measured metrics. The result shows a significant age-related decrease in mean diameter of the blood vessel ($t(12) = 2.9034$, p-value = 0.0132) in 9 samples of older adults ($M = 3.5686$, $SD = 0.1103$) as compared to 5 samples of young adults ($M = 3.7929$, $SD = 0.1822$). There has not been a statistically significant difference in vessel density, vessel perimeter index and vessel length density (p-value > 0.05) with age as the person suffers from cognitive decline due to CSVD or Alzheimer's because of the following reasons: a) The decrease in the vessel density as presented in the literature review has been associated with a decline in cognitive ability due to CSVD or Alzheimer's. However, the older individual's dataset, ROSE-1 contained images from older individuals with Alzheimer's as well as control group (of older people but not suffering with Alzheimer's) which must be affecting the results. Please note that, the categorization of the images as to which image belongs to which group in the ROSE-1 dataset has not been revealed yet. Hence, the complete dataset of older people containing images from control group and people suffering from Alzheimer's was used. b) Both the datasets compared, were captured from different OCTA imaging device, although there is a very low chance of this affecting the results, this might be one of the factors affecting it.

This section described an overview of what was presented in the thesis with some descriptions of the observations made. The next three section will summarize the contributions made through this research, its limitations, and the road map to the future work.

5.1 Contributions

Even after recent growth in the studies working on the segmentation of OCTA images and its use in evaluating the effect of diseases like CSVD and Alzheimer's on the retinal vasculature, there is a lack of standardized segmentation technique mostly because of the absence of publicly available dataset. Hence, this research builds on the first ever published dataset [1] with the pixel-level and

centerline manual annotations. Additionally, this study included training and acquisition of OCTA images of younger individuals for comparison.

A novel SVC segmentation approach has also been proposed using Attention UNet model as a base model with promising results. The Attention UNet trained model (over ROSE-1 dataset) was also used to segment the thicker blood vessels in the NCM images successfully (even though it was captured from a different device). Furthermore, the thicker blood vessels from both the datasets were analyzed by extracting the vascular features and statistically analyzing them. Hence, revealing some information about the changes that occurs in the brain with ageing and cognitive decline.

5.2 Limitations

Although the findings of this research are crucial in the field of OCTA segmentation and using it as a tool to study the changes in the brain due to cognitive decline, there are a few limitations presented as follows:

a) The absence of the information about which image belonged to which group in the OCTA image dataset ROSE-1. With that information, a direct comparison of the vascular features can be made in between the control group and the Alzheimer's group. Another comparison can be made in between the vascular features from OCTA between younger individuals' images (collected at University of Ottawa) and the Alzheimer's group. This could help in development of biomarkers aiding in the early detection of Alzheimer's.

b) The dataset used namely: ROSE-1 and NCM images were captured with two different OCTA machine. Although, this should not cause any major differences, as the images of interest were both SVC OCTA images.

c) While capturing OCTA scans at the University of Ottawa, several individuals provide the scans as they were sensitive to the light in the OCTA device. Hence, limiting the images

captured. Furthermore, it might be even more difficult for older individuals with cognitive decline to proceed with the OCTA scans.

d) The absence of ground truth images of OCTA scans captured in the NCM lab did not allow to analyse the effect of different preprocessing methods on OCTA images captured from Heidelberg OCTA system (NCM images). This resulted in inconsistent preprocessing methods for ROSE dataset and NCM dataset which is important for automation.

e) As this study was conducted during the period of COVID lockdown, it was a challenge to collect scans of more people in the NCM lab resulting in a limited image in NCM dataset which is why this study was relied on ROSE dataset.

5.3 Future Work

The work presented in this report can be proceeded in various directions. Firstly, once the authors of Ma Y. et al. [1] publishes the classification of images into controls and Alzheimer's, the ROSE-1 dataset can be used to study the vascular changes in between the two groups. Extracted features can be fed into a machine learning algorithm which can classify images as diseased (Alzheimer's group) and control. This will give a better idea of which features are more important.

Another direction is to acquire more images and develop a complete dataset with manual annotations of older people group and younger individuals at the lab of University of Ottawa. This can be assisted with corresponding MRI images as well so that a link can be established in between the brain changes observed in the MRI scans and the vascular changes in the OCTA images.

For the proposed segmentation approach, it would've worked even better if there were more images to train the Attention UNet model. It has shown great promise in segmenting images with higher accuracy even with smaller number of training images. Therefore, if the model is trained with OCTA images captured from different devices, then it will be able to segment the data from any device with even better evaluation metrics.

Hessian matrix are widely used in highlighting tube like structures such as fibers or vessels in medical images. The use of Hessian matrix as a preprocessing step can be studied for images captured by both the OCTA devices (RTVue XR Avanti SD-OCT system and Heidelberg OCT2 system).

Develop a robust preprocessing method which can deal with images captured from different OCTA systems. This is important especially while automating the process of segmentation of OCTA images where the input can be an OCTA scan captured from any device and the output is a segmented image. Hence, it becomes important to make the pre-processing consistent for all types of OCTA images.

REFERENCES

[1] Y. Ma *et al.*, "ROSE: A Retinal OCT-Angiography Vessel Segmentation Dataset and New Model," *IEEE Trans. Med. Imaging*, vol. 40, no. 3, pp. 928–939, 2021, doi: 10.1109/TMI.2020.3042802.

[2] X. Zhang *et al.*, "Optical Coherence Tomography Angiography Reveals Distinct Retinal Structural and Microvascular Abnormalities in Cerebrovascular Disease," *Front. Neurosci.*, vol. 14, no. October, pp. 1–9, 2020, doi: 10.3389/fnins.2020.588515.

[3] A. London, I. Benhar, and M. Schwartz, "The retina as a window to the brain - From eye research to CNS disorders," *Nat. Rev. Neurol.*, vol. 9, no. 1, pp. 44–53, 2013, doi: 10.1038/nrneurol.2012.227.

[4] J. Zhang, L. Shi, and Y. Shen, "The retina: A window in which to view the pathogenesis of Alzheimer's disease," *Ageing Res. Rev.*, vol. 77, no. August 2021, p. 101590, 2022, doi: 10.1016/j.arr.2022.101590.

[5] Y. Zhang, X. Zhang, Y. Yue, and T. Tian, "Retinal Degeneration: A Window to Understand the Origin and Progression of Parkinson's Disease?," *Front. Neurosci.*, vol. 15, no. February, 2022, doi: 10.3389/fnins.2021.799526.

[6] P. Zabel *et al.*, "Comparison of retinal microvasculature in patients with Alzheimer's disease and primary open-angle glaucoma by optical coherence tomography angiography," *Investig. Ophthalmol. Vis. Sci.*, vol. 60, no. 10, pp. 3447–3455, 2019, doi: 10.1167/IOVS.19-27028.

[7] Y. Zhang, Y. Wang, C. Shi, M. Shen, and F. Lu, "Advances in retina imaging as potential biomarkers for early diagnosis of Alzheimer's disease," *Transl. Neurodegener.*, vol. 10, no. 1, pp. 1–9, 2021, doi: 10.1186/s40035-021-00230-9.

[8] S. M. Langner *et al.*, "Structural retinal changes in cerebral small vessel disease," *Sci.*

Rep., vol. 12, no. 1, pp. 1–10, 2022, doi: 10.1038/s41598-022-13312-z.

[9] O. M. Rifai, S. McGroy, C. B. Robbins, D. S. Grewal, A. Liu, and S. Fekrat, "The application of optical coherence tomography angiography in Alzheimer's disease:A systematic review," *Diagnosis, Assess. Dis. Monit.*, 2021, doi: 0.1002/dad2.12149.

[10] J. F. Zhang *et al.*, "The Application of Optical Coherence Tomography Angiography in Cerebral Small Vessel Disease, Ischemic Stroke, and Dementia: A Systematic Review," *Front. Neurol.*, vol. 11, no. September, pp. 1–12, 2020, doi: 10.3389/fneur.2020.01009.

[11] Q. Li *et al.*, "Cerebral Small Vessel Disease," *Cell Transplant.*, vol. 27, no. 12, pp. 1711–1722, 2018, doi: 10.1177/0963689718795148.

[12] J. Chojdak-Łukasiewicz, E. Dziadkowiak, A. Zimny, and B. Paradowski, "Cerebral small vessel disease: A review," *Adv. Clin. Exp. Med.*, vol. 30, no. 3, pp. 349–356, 2021, doi: 10.17219/ACEM/131216.

[13] van N. A.G.W. *et al.*, "Causes and consequences of cerebral small vessel disease. The RUN DMC study: A prospective cohort study. Study rationale and protocol.," *BMC Neurol.*, vol. 11, p. no pagination, 2011.

[14] S. H. Kreisel *et al.*, "Deterioration of gait and balance over time: The effects of age-related white matter change - The LADIS study," *Cerebrovasc. Dis.*, vol. 35, no. 6, pp. 544–553, 2013, doi: 10.1159/000350725.

[15] S. Debetter and H. S. Markus, "The clinical importance of white matter hyperintensities on brain magnetic resonance imaging: systematic review and meta-analysis," *BMJ*, 2010, doi: https://doi.org/10.1136/bmj.c3666.

[16] M. L. Callisaya, R. Beare, T. G. Phan, A. G. Thrift, and V. K. Srikanth, "Brain Structural Change and Gait Decline: A Longitudinal Population-Based Study," *J. Am. Geriatr. Soc.*, 2013.

[17] W. M. van der Flie, W. van Straaten, F. Barkhof, A. Verdelho, and S. Madureira, "Small

Vessel Disease and General Cognitive Function in Nondisabled Elderly," *Am. Hear. Assoc.*, 2005.

[18] I. López-Cuenca *et al.*, "The relationship between retinal layers and brain areas in asymptomatic first-degree relatives of sporadic forms of Alzheimer's disease: an exploratory analysis," *Alzheimers. Res. Ther.*, vol. 14, no. 1, pp. 1–18, 2022, doi: 10.1186/s13195-022-01008-5.

[19] C. M and M. Das J., *Anatomy, Head and Neck, Internal Carotid Arteries*. StatPearls Publishing, 2022.

[20] A. Balasopoulou *et al.*, "Symposium Recent advances and challenges in the management of retinoblastoma Globe - saving Treatments," *BMC Ophthalmol.*, vol. 17, no. 1, p. 1, 2017, doi: 10.4103/ijo.IJO.

[21] P. K. Kaiser *et al.*, "Retinal Fluid and Thickness As Measures of Disease Activity in Neovascular Age-Related Macular Degeneration," *Retina*, vol. 41, no. 8, pp. 1579–1586, 2021, doi: 10.1097/IAE.0000000000003194.

[22] J. S. Schuman, "Spectral domain optical coherence tomography for glaucoma (an AOS thesis)," *Trans. Am. Ophthalmol. Soc.*, vol. 106, pp. 426–458, 2008.

[23] A. H. Kashani *et al.*, "Optical coherence tomography angiography: A comprehensive review of current methods and clinical applications," *Prog. Retin. Eye Res.*, vol. 60, pp. 66–100, 2017, doi: 10.1016/j.preteyeres.2017.07.002.

[24] G. Wildeman and H. Dhalla, "Leica Microsystems." https://www.leica-microsystems.com/science-lab/what-is-oct-and-how-can-it-help-ophthalmologists-acquire-high-resolution-information-on-ocular-tissue/.

[25] A. Wylęgała, "Principles of OCTA and Applications in Clinical Neurology," *Curr. Neurol. Neurosci. Rep.*, vol. 18, no. 12, 2018, doi: 10.1007/s11910-018-0911-x.

[26] J. P. Campbell *et al.*, "Detailed Vascular Anatomy of the Human Retina by Projection-

Resolved Optical Coherence Tomography Angiography," *Sci. Rep.*, vol. 7, no. September 2016, pp. 1–11, 2017, doi: 10.1038/srep42201.

[27] "Heilderberg Engineering." https://business-lounge.heidelbergengineering.com/us/en/news/news/know-your-retinal-layers-33401465.

[28] M. Bulut *et al.*, "Evaluation of optical coherence tomography angiographic findings in Alzheimer's type dementia," *Br. J. Ophthalmol.*, vol. 102, no. 2, pp. 233–237, 2018, doi: 10.1136/bjophthalmol-2017-310476.

[29] S. P. Yoon. *et al.*, "Retinal microvascular and neurodegenerative changes in Alzheimer's disease and mild cognitive impairment compared to controls," *Physiol. Behav.*, vol. 176, no. 3, pp. 139–148, 2017, doi: 10.1016/j.oret.2019.02.002.Retinal.

[30] H. Jiang *et al.*, "Altered macular microvasculature in mild cognitive impairment and Alzheimer disease," *J. Neuro-Ophthalmology*, vol. 38, no. 3, pp. 292–298, 2018, doi: 10.1097/WNO.0000000000000580.

[31] J. Wu, X. Zhang, G. Azhati, T. Li, G. Xu, and F. Liu, "Retinal microvascular attenuation in mental cognitive impairment and Alzheimer's disease by optical coherence tomography angiography," *Acta Ophthalmol.*, vol. 98, no. 6, pp. e781–e787, 2020, doi: 10.1111/aos.14381.

[32] J. A. Van De Kreeke *et al.*, "Optical coherence tomography angiography in preclinical Alzheimer's disease," *Br. J. Ophthalmol.*, pp. 157–161, 2019, doi: 10.1136/bjophthalmol-2019-314127.

[33] J. den Haan *et al.*, "Is retinal vasculature a biomarker in amyloid proven Alzheimer's disease?," *Alzheimer's Dement. Diagnosis, Assess. Dis. Monit.*, vol. 11, pp. 383–391, 2019, doi: 10.1016/j.dadm.2019.03.006.

[34] G. Querques *et al.*, "Functional and morphological changes of the retinal vessels in Alzheimer's disease and mild cognitive impairment," *Sci. Rep.*, vol. 9, no. 1, pp. 1–10,

2019, doi: 10.1038/s41598-018-37271-6.

[35] L. Lahme, E. L. Esser, N. Mihailovic, F. Schubert, J. Lauermann, and A. Johen, "Evaluation of Ocular Perfusion in Alzheimer's Disease Using Optical Coherence Tomography Angiography," *J. Alzheimer's Dis.*, 2018.

[36] Y. S. Zhang *et al.*, "Parafoveal vessel loss and correlation between peripapillary vessel density and cognitive performance in amnestic mild cognitive impairment and early Alzheimer's Disease on optical coherence tomography angiography," *PLoS One*, vol. 14, no. 4, pp. 1–16, 2019, doi: 10.1371/journal.pone.0214685.

[37] M. Alam, D. Thapa, J. I. Lim, D. Cao, and X. Yao, "Quantitative characteristics of sickle cell retinopathy in optical coherence tomography angiography," *Biomed. Opt. Express*, vol. 8, no. 3, p. 1741, 2017, doi: 10.1364/boe.8.001741.

[38] M. Alam, D. Toslak, J. I. Lim, and X. Yao, "OCT feature analysis guided artery-vein differentiation in OCTA," *Biomed. Opt. Express*, vol. 10, no. 4, p. 2055, 2019, doi: 10.1364/boe.10.002055.

[39] K. Pappelis and N. M. Jansonius, "Quantification and repeatability of vessel density and flux as assessed by optical coherence tomography angiography," *Transl. Vis. Sci. Technol.*, vol. 8, no. 3, 2019, doi: 10.1167/tvst.8.3.3.

[40] J. H. Terheyden, M. W. M. Wintergerst, P. Falahat, M. Berger, F. G. Holz, and R. P. Finger, "Automated thresholding algorithms outperform manual thresholding in macular optical coherence tomography angiography image analysis," *PLoS One*, vol. 15, no. 3, pp. 1–12, 2020, doi: 10.1371/journal.pone.0230260.

[41] O. Aharony, O. Gal-Or, A. Polat, Y. Nahum, D. Weinberger, and Y. Zimmer, "Automatic characterization of retinal blood flow using oct angiograms," *Transl. Vis. Sci. Technol.*, vol. 8, no. 4, pp. 0–9, 2019, doi: 10.1167/tvst.8.4.6.

[42] X. Xu *et al.*, "Automated quantification of superficial retinal capillaries and large vessels

for diabetic retinopathy on optical coherence tomographic angiography," *J. Biophotonics*, vol. 12, no. 11, pp. 1–8, 2019, doi: 10.1002/jbio.201900103.

[43] S. Wu *et al.*, "An optimized segmentation and quantification approach in microvascular imaging for OCTA-based neovascular regression monitoring," *BMC Med. Imaging*, vol. 21, no. 1, pp. 1–9, 2021, doi: 10.1186/s12880-021-00546-y.

[44] D. Andrade De Jesus *et al.*, "OCTA multilayer and multisector peripapillary microvascular modeling for diagnosing and staging of glaucoma," *Transl. Vis. Sci. Technol.*, vol. 9, no. 2, pp. 1–22, 2020, doi: 10.1167/tvst.9.2.58.

[45] K. M. Meiburger *et al.*, "Automatic skin lesion area determination of basal cell carcinoma using optical coherence tomography angiography and a skeletonization approach: Preliminary results," *J. Biophotonics*, vol. 12, no. 9, pp. 1–11, 2019, doi: 10.1002/jbio.201900131.

[46] J. Zhang *et al.*, "3D Shape Modeling and Analysis of Retinal Microvasculature in OCT-Angiography Images," *IEEE Trans. Med. Imaging*, vol. 39, no. 5, pp. 1335–1346, 2020, doi: 10.1109/TMI.2019.2948867.

[47] L. Su *et al.*, "Quantitative assessment of the retinal microvasculature and choriocapillaris in myopic patients using swept-source optical coherence tomography angiography," *Graefe's Arch. Clin. Exp. Ophthalmol.*, vol. 258, no. 6, pp. 1173–1180, 2020, doi: 10.1007/s00417-020-04639-2.

[48] E. Borrelli, R. Sacconi, L. Querques, M. Battista, F. Bandello, and G. Querques, "Quantification of diabetic macular ischemia using novel three-dimensional optical coherence tomography angiography metrics," *J. Biophotonics*, vol. 13, no. 10, pp. 1–10, 2020, doi: 10.1002/jbio.202000152.

[49] Z. Chu *et al.*, "Quantitative assessment of the retinal microvasculature using optical coherence tomography angiography," *J. Biomed. Opt.*, vol. 21, no. 6, p. 066008, 2016,

doi: 10.1117/1.jbo.21.6.066008.

[50] A. Y. Kim, Z. Chu, A. Shahidzadeh, R. K. Wang, C. A. Puliafito, and A. H. Kashani, "Quantifying microvascular density and morphology in diabetic retinopathy using spectral-domain optical coherence tomography angiography," *Investig. Ophthalmol. Vis. Sci.*, vol. 57, no. 9, pp. OCT362–OCT370, 2016, doi: 10.1167/iovs.15-18904.

[51] N. Mehta *et al.*, "Repeatability of binarization thresholding methods for optical coherence tomography angiography image quantification," *Sci. Rep.*, vol. 10, no. 1, pp. 1–11, 2020, doi: 10.1038/s41598-020-72358-z.

[52] M. M. Khansari, W. O'Neill, J. Lim, and M. Shahidi, "Method for quantitative assessment of retinal vessel tortuosity in optical coherence tomography angiography applied to sickle cell retinopathy," *Biomed. Opt. Express*, vol. 8, no. 8, p. 3796, 2017, doi: 10.1364/boe.8.003796.

[53] J. Cano *et al.*, "Classification of advanced and early stages of diabetic retinopathy from non-diabetic subjects by an ordinary least squares modeling method applied to OCTA images," *Biomed. Opt. Express*, vol. 11, no. 8, p. 4666, 2020, doi: 10.1364/boe.394472.

[54] J. Xue *et al.*, "Unsupervised Segmentation of Choroidal Neovascularization for Optical Coherence Tomography Angiography by Grid Tissue-Like Membrane Systems," *IEEE Access*, vol. 7, pp. 143058–143066, 2019, doi: 10.1109/ACCESS.2019.2943186.

[55] A. M. E. Engberg, V. A. Dahl, and A. B. Dahl, "Dictionary-based Method for Vascular Segmentation for OCTA Images," vol. i, pp. 1–11, 2020, [Online]. Available: http://arxiv.org/abs/2002.03945.

[56] H. E. Kim, A. Cosa-Linan, N. Santhanam, M. Jannesari, M. E. Maros, and T. Ganslandt, "Transfer learning for medical image classification: a literature review," *BMC Med. Imaging*, vol. 22, no. 1, pp. 1–13, 2022, doi: 10.1186/s12880-022-00793-7.

[57] K. He, X. Zhang, S. Ren, and Jian Sun, "Deep Residual Learning for Image Recognition,"

Proc. IEEE Conf. Comput. Vis. Pattern Recognition, pp. 770–778, 2016, doi: 10.1002/chin.200650130.

[58] Y. Giarratano *et al.*, "Automated segmentation of optical coherence tomography angiography images: Benchmark data and clinically relevant metrics," *Transl. Vis. Sci. Technol.*, vol. 9, no. 13, pp. 1–10, 2020, doi: 10.1167/tvst.9.13.5.

[59] J. Lo *et al.*, "Microvasculature segmentation and intercapillary area quantification of the deep vascular complex using transfer learning," *Transl. Vis. Sci. Technol.*, vol. 9, no. 2, pp. 1–12, 2020, doi: 10.1167/tvst.9.2.38.

[60] T. Pissas *et al.*, "Deep iterative vessel segmentation in OCT angiography," *Biomed. Opt. Express*, vol. 11, no. 5, p. 2490, 2020, doi: 10.1364/boe.384919.

[61] S. Yu *et al.*, "3D vessel reconstruction in OCT-Angiography via depth map estimation," *Proc. Int. Symp. Biomed. Imaging*, pp. 1609–1613, 2021.

[62] Y. Guo *et al.*, "Development and validation of a deep learning algorithm for distinguishing the nonperfusion area from signal reduction artifacts on OCT angiography," *Biomed. Opt. Express*, vol. 10, no. 7, p. 3257, 2019, doi: 10.1364/boe.10.003257.

[63] M. Li *et al.*, "Image Projection Network: 3D to 2D Image Segmentation in OCTA Images," *IEEE Trans. Med. Imaging*, vol. 39, no. 11, pp. 3343–3354, 2020, doi: 10.1109/TMI.2020.2992244.

[64] M. Li *et al.*, "IPN-V2 and OCTA-500: Methodology and Dataset for Retinal Image Segmentation," no. 2, pp. 1–12, 2020, [Online]. Available: http://arxiv.org/abs/2012.07261.

[65] T. P. Das, S. Praharaj, S. Swain, S. Agarwal, and K. Kumar, "Application of Top-hat Transformation for Enhanced Blood Vessel Extraction," 2022, [Online]. Available: http://arxiv.org/abs/2203.10005.

[66] H. Zhang *et al.*, "ResNeSt: Split-Attention Networks," 2020, [Online]. Available:

http://arxiv.org/abs/2004.08955.

[67] O. Ronneberger, P. Fischer, and T. Brox, “U-Net: Convolutional Networks for Biomedical Image Segmentation,” *Springer Int.*, vol. 9351, no. Cvd, pp. 12–20, 2015, doi: 10.1007/978-3-319-24574-4.

[68] O. Oktay *et al.*, “Attention U-Net: Learning Where to Look for the Pancreas,” no. Midl, 2018, [Online]. Available: http://arxiv.org/abs/1804.03999.

[69] V. Pramil, E. S. Levine, and N. K. Waheed, “Macular vessel density in diabetic retinopathy patients: How can we accurately measure and what can it tell us?,” *Clin. Ophthalmol.*, vol. 15, pp. 1517–1527, 2021, doi: 10.2147/OPTH.S272328.

[70] P. Guimarães, J. Wigdahl, and A. Ruggeri, “A fast and efficient technique for the automatic tracing of corneal nerves in confocal microscopy,” *Transl. Vis. Sci. Technol.*, vol. 5, no. 5, 2016, doi: 10.1167/tvst.5.5.7.

Appendix A

- **Structural element of Top Hat filter**: The shape and size of the structural element for the top hat filter was decided based on the trial-and-error method. Different structural elements were studied including diamond, line, and rectangle of different size. The best results were obtained using a square as the structural element as it provided with an OCTA scan where the background noise was most suppressed, and the Region of Interest was enhanced.
- **Median filter window size:** Median filtering is used to smoothen the spike noise while preserving the edges. The decision of its window size was based on trial-and-error method. A window size of 5*5 was leading to a blurrier image which was not desirable for the segmentation of blood vessels. The optimal result was obtained by using a window size of 3*3, which has been used in this research.
- The decision to include the preprocessing steps in the process of segmentation was because these pre-processing steps led to enhancement of the raw OCTA scans and led to better segmentation of blood vessels. Even with a simpler segmentation technique such as UNET the segmentation of blood vessels had an increased accuracy of 0.9312 as compared 0.8955 without pre-processing. The DICE coefficient also increased from 0.7116 to 0.7578 when the pre-processing steps were included in segmentation.